이학석사 학위논문

높은 안정성과 광학 특성을 지닌 전도성 고분자 코팅된 귀금속 나노삼각형의 제조

Fabrication of Conjugated Polymer-Coated Noble-Metal Nanoprisms with High Stability and Optical Properties

2017 년 2 월

서울대학교 대학원

화학부 물리화학 전공

정 수 경

A Master's Dissertation

Fabrication of Conjugated Polymer-Coated Noble-Metal Nanoprisms with High Stability and Optical Properties

by Sugyeong Jeong

Supervisor: Professor Du-Jeon Jang

Major: Physical Chemistry

Department of Chemistry

Graduate School of

Seoul National University

February 2017

Abstract of Dissertation

The fabrication, characterization, stability, and optical properties of conjugated polymer-coated noble-metal nanoprisms are discussed from the point of view of physical and materials chemistry. Brief overviews of the chapter 1 and 2 in this dissertation are shown below.

In chapter 1, silver nanoprisms (Ag-PRs) have been expitaxially edge-coated with gold and subsequently covered fully with P3HT chains to fabricate poly(3-hexylthiophene)-grafted edge-gold-coated silver nanoprisms (P3HT@AuAg-PRs) which are miscible with organic solvents. Both absorption and emission spectra have indicated that aggregated P3HT chains are bound on the surfaces of noble-metal nanoprisms. Picosecond emission kinetic profiles have suggested that the S_1 relaxation time of P3HT in P3HT@AuAg-PRs is reduced due to energy transfer to AuAg-PRs. From nanosecond transient-absorption kinetic profiles, the reduced amplitude and the increased decay time of T_1 excitons in P3HT@AuAg-PRs have been measured. The surface-enhanced Raman scattering effect of P3HT@AuAg-PRs is as high as 4.6 because the sharp tips of AuAg-PRs which are maintained via gold coating serve as “hot spots”. The morphology deformation time of P3HT@AuAg-PRs in H_2O_2(aq) has been extended 48 times longer than that of Ag-PRs.

In chapter 2, self-assemblies of silver nanoprisms (AgPRs) having enhanced structural stability and optical properties have been facilely coated with polypyrrole (PPy) *via* the *in situ* polymerization of pyrrole (Py) monomers that also act as an assembling agent. The degree of AgPRs assembly has been controlled by varying the concentrations of trisodium citrate dihydrate, which bind selectively to the {111} facets of AgPRs. The morphology deformation time of self-assembled AgPRs just with thin PPy coating is 7 times longer than that of PPy-free AgPRs, suggesting that PPy coating prevents the sharp tips of AgPRs from being truncated by oxidizing agents. The surface-enhanced Raman scattering effect of highly assembled and

PPy-coated AgPRs becomes as high as 6.3 due to the well-maintained sharp tips of AgPRs by PPy coating, as well as numerous hot spots generated between nanoprisms.

Keywords:

Conjugated polymer, Noble-metal, Optical properties, Raman scattering, Self-assembly, Silver nanoprisms, Stability

Student Number: 2014-21225

Contents

List of Figures and Tables

best-fitted curves.

Figure 1-9. Raman spectra of pristine P3HT, P3HT@Ag-PRs, and P3HT@AuAg-PRs. The concentration of P3HT was fixed and all the samples were excited at 532 nm.

Figure 1-10. Absorption spectral evolutions of (a) Ag-PRs and (b) AuAg-PRs dispersed in water and (c) P3HT@AuAg-PRs dispersed in THF after treatment with H_2O_2. (d) A/A_0 vs t at 804 nm for Ag-PRs, 823 nm for AuAg-PRs, and 998 nm for P3HT@AuAg-PRs.

Figure 1-S1. TEM images of (a) Ag-PRs and (b) AuAg-PRs.

Figure 1-S2. EDX analysis spectrum of P3HT@AuAg-PRs, where the molar percentages of silver, gold, and sulfur have been observed to be 88.8%, 8.7%, and 2.5%, respectively.

Figure 1-S3. Absorption spectra of Ag-PRs and AuAg-PRs dispersed in water.

Figure 1-S4. TEM image of P3HT@AuAg-PRs and hot spots marked with yellow-dotted circles.

Table 1-1. Fluorescence and transient-absorption decay constants of P3HT and P3HT@AuAg-PRs in THF.

Table 1-S1. Binding energies in eV for the deconvoluted curves of S 2p XPS spectra.

Table 1-S2. Binding energies in eV for the deconvoluted curves of Ag 3d and Au 4f XPS spectra.

Table 1-S3. Spectral positions of four Gaussian curves extracted from the subtracted absorption spectrum of Figure 5b.

Table 1-S4. Half lifetimes ($t_{1/2}$) for the morphology deformation of nanoprisms via H_2O_2.

Figure 2-1. Schematically presented PPy coating of self-assembled AgPRs on the surfaces of AgPRs, depending on the concentration of TSC. Blue and red colors represent silver and PPy, respectively.

Figure 2-2. High-resolution TEM images for (a) PPy-free AgPRs and PPy-coated AgPRs of (b) AgPRs/TSC-0, (c) AgPRs/TSC-5, (d) AgPRs/TSC-10, (e) AgPRs/TSC-50, and (f) AgPRs/TSC-100.

Figure 2-3. Absorption spectra of (a) AgPRs in the absence of Py and (b) AgPRs/TSC-0, (c) AgPRs/TSC-10, and (d) AgPRs/TSC-100 in the presence of Py, recorded as a function of time after diluting AgPRs colloids in water.

Figure 2-4. Absorption spectra of (black) PPy-free AgPRs and PPy-coated AgPRs of (blue) AgPRs/TSC-0, (green) AgPRs/TSC-5, (orange) AgPRs/TSC-10, (purple) AgPRs/TSC-50, and (red) AgPRs/TSC-100 dispersed in water.

Figure 2-5. FTIR spectra of PPy-free AgPRs, pristine PPy, and PPy-coated AgPRs/TSC-100: (1) C=O stretching at 1726 cm^{-1}, (2) N–H bending at 1536 cm^{-1}, and (4) C–N stretching at 1164 cm^{-1}.

Figure 2-6. Absorption spectral evolutions of (a) PPy-free AgPRs and (b) PPy-coated AgPRs/TSC-100 after treatment with H_2O_2(aq) for periods indicated in the units of min.

Figure 2-7. $\ln(A/A_0)$ vs *t* after treatment with H_2O_2(aq), monitored at 833 nm for PPy-free AgPRs and 935 nm for PPy-coated AgPRs/TSC-100.

Figure 2-8. Raman spectra of 4MBA on (black) glass, (blue) PPy-free AgPRs, (gree) PPy-coated (green) AgPRs/TSC-0, and (red) PPy-coated AgPRs/TSC-100 substrates with excitation at 532 nm.

Figure 2-S1. Low-resolution TEM images (left) and assembly-degree histograms (right) of (a) AgPRs/TSC-0, (b) AgPRs/TSC-5, (c) AgPRs/TSC-10, (d) AgPRs/TSC-50, and (e) AgPRs/TSC-100.

Figure 2-S2. TEM images of AgPRs/TSC-100 aged for (a) 1, (b) 2, (c) 3, and (d) 7 days in the presence of Py. Note that each sample was dispersed in ethanol prior to TEM loading.

Figure 2-S3. Absorption spectra of PPy-free AgPRs in (black) water and (red) ethanol. The inset TEM image shows PPy-free AgPRs, which were dispersed in ethanol prior to TEM loading.

Chapter 1. Colloidal System of Polythiophene-Grafted Edge-Gold-Coated Silver Nanoprisms with Enhanced Optical Properties and Stability

1.1. Abstract

Silver nanoprisms (Ag-PRs) have been expitaxially edge-coated with gold and subsequently covered fully with P3HT chains to fabricate poly(3-hexylthiophene)-grafted edge-gold-coated silver nanoprisms (P3HT@AuAg-PRs) which are miscible with organic solvents; each AuAg-PR with a typical edge length of 122 nm is surrounded by 4.4 x 10^3 P3HT chains. Both absorption and emission spectra have indicated that aggregated P3HT chains are bound on the surfaces of noble-metal nanoprisms. Picosecond emission kinetic profiles have suggested that the S_1 relaxation time of P3HT in P3HT@AuAg-PRs is reduced due to energy transfer to AuAg-PRs. From nanosecond transient-absorption kinetic profiles, the reduced amplitude and the increased decay time of T_1 excitons in P3HT@AuAg-PRs have been measured, indicating that neither the intersystem crossing of S_1 into T_1 nor the intersystem crossing of T_1 into S_0 occurs effectively in P3HT@AuAg-PRs owing to the stretched and rigid conformations of P3HT chains bound on the surfaces of AuAg-PRs. The surface-enhanced Raman scattering effect of P3HT@AuAg-PRs is as high as 4.6 because the sharp tips of AuAg-PRs which are maintained via gold coating serve as “hot spots”. The morphology deformation time of P3HT@AuAg-PRs in H_2O_2(aq) has been extended 48 times longer than that of Ag-PRs. Overall, our fabricated nanocomposites of P3HT@AuAg-PRs not only have feasible-process ability but also possess enhanced optical properties and high stability against oxidizing agents, extending the use of noble-metal nanoprisms for various optical applications.

1.2. Introduction

Colloidal noble-metal nanoparticles have been the focus of intense study for applications in catalysis, surface-enhanced Raman scattering (SERS), biosensors, and plasmonics because of their unique plasmonic properties, which originate from light absorption and scattering by the localized surface-plasmon resonance (LSPR) [1-5]. LSPR, which is caused by the collective oscillation of electrons in the conduction band of a metal, can be excited by visible or near-infrared light and its resonance frequency is highly dependent on the shape and size of the metal [6]. Among all the noble metals, silver is well known to exhibit superior optical properties such as high LSPR sensitivities and strong field enhancement [7,8]. Thus, much effort has been devoted to synthesize silver nanoparticles with shapes varying from spheres to cubes, polyhedrons, plates, and wires, dramatically broadening the range of the LSPR wavelength [9]. Particularly, the fabrication of silver nanoprisms (Ag-PRs) with controlled sizes has been explored extensively [10]. Typically, Ag-PR has three sharp vertices, which lead to strong near-field enhancement by the lightning-rod effect [11], making Ag-PRs useful for plasmonic applications such as SERS, metal-enhanced fluorescence, and plasmon-enhanced organic electronic devices [12]. Despite such advantages, the utility of Ag-PR is limited because the vertices of Ag-PR are unstable and susceptible to truncation over time when they are exposed to water, halides, UV-irradation, and heat, resulting in broadening and blue shift of the LSPR band accompanied with a loss of surface-plasmon intensity [13,14].

A number of researches have reported the protection of Ag-PR [15-17]. For example, Du *et al*. have employed a protecting layer of TiO_2 or SiO_2 to coat the surface of Ag-PR, preventing the edges of Ag-PR from truncation over time [16]. Xue *et al*. have incorporated 16-mercaptohexadecanoic acid for the stabilization of Ag-PR against etching by silica coating [17].

However, difficult control over the oxide-layer thickness and less sensitive LSPR of Ag-PR limit the usefulness of the nanoprisms. Other groups have used gold to ensure the stability of Ag-PR while maintaining shape asperities and optical properties such as high electric-field distribution around the nanoprisms [7,8]. Coating Ag-PR with less reactive noble metals such as gold has been investigated not only to protect against disturbance from the environment over a long period but also to keep the orginal plasmonic property and surface characteristics of Ag-PR. However, the dispersion of nanoprisms is still exclusively limited in aqueous media. Since many applications require nanoprisms to be blended or well dispersed into the host organic materials, it is crucial to make them miscible with organic solvents, thus, maximizing the utility of Ag-PRs [18,19].

Recently, conjugated polymers have often been incorporated not only to protect metal nanoparticles from corrosion, chemical poisoning, and dissolution but also to make them miscible in organic media [20-27]. Particularly, hybrid materials containing conjugated polymers and Ag-PRs are widely used for organic photovoltaic (OPV) devices having enhanced chemical and physical properties, which are not found from single-component counterparts. For example, Kulkarni *et al*. have used Ag-PRs as optical antennas and scattering centers for OPV devices and investigated the optical properties of conjugated polymer-based cells having Ag-PRs in the film condition [28]. Shahjamali *et al*. have also reported that the performance of an OPV cell was enhanced when the bulk heterojunction film of poly(3-hexylthiophene)/phenyl-C61-butyric acid methiyl ester (P3HT/PCBM) was spin-coated on the glass substrate that had been immersed in a colloidal solution of edge-gold-coated silver nanoprisms [29]. They have suggested that highly stable edge-gold-coated silver nanoprisms act as optical antennas to enhance incident-light absorption in the active layer of OPV devices [29]. Likewise, interactions between the plasmon resonance of Ag-PR and the exciton of

conjugated polymers have been extensively explored by using various optical instruments; however, the study is often limited to the film state of these two materials so the profound study on the optical properties of such hybrid systems in the colloidal state should be essential for the fundamental understanding of these nanocomposites.

In this paper, we have fabricated poly(3-hexylthiophene)-grafted edge-gold-coated silver nanoprisms (P3HT@AuAg-PRs) by blending thiol-functionalized P3HT (P3HT-SH) in tetrahydrofuran (THF) with edge-gold-coated silver nanoprisms (AuAg-PRs) dispersed in water (Figure 1-1) and investigated their optical properties and stability in the colloidal state. As-prepared P3HT@AuAg-PRs are miscible well with organic solvents and have enhanced optical properties such as high SERS effect. The extremely extended deformation time of P3HT@AuAg-PRs in H_2O_2(aq) has demonstrated their highly improved stability, extending the use of noble-metal nanoprisms for various optical applications.

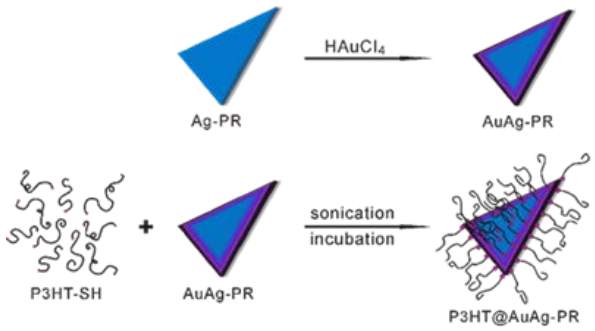

Figure 1-1. Scheme for the fabrication of a thiol-functionalized P3HT-grafted edge-gold-coated silver nanoprism (P3HT@AuAg-PR).

1.3. Experimental Section

Chemicals. Chemicals were used as received: gold chloride trihydrate ($HAuCl_4 \bullet 3H_2O$), silver nitrate ($AgNO_3$), L-ascorbic acid, sodium borohydride ($NaBH_4$), and trisodium citrate dihydrate (TSC, $Na_3C_6H_5O_7 \bullet 2H_2O$) from Sigma-Aldrich; acetonitrile from Ducksan Pharmaceutical; 34% H_2O_2(aq) from Samchun Pure Chemicals; and THF from Daejung Chemicals & Metals. Ultrapure deionized water (>15 MΩ cm) from an Elga PURELAB option-S system was used throughout the experiments.

Synthesis of Ag-PRs and AuAg-PRs. Ag-PRs were synthesized *via* a seed-mediated growth method [30] with some modifications. Briefly, the silver seed solution was prepared by dissolving 12 mL of 75 mM TSC(aq), 0.20 mL of 0.10 M $AgNO_3$(aq) and 0.42 mL of 34% H_2O_2(aq) in 200 mL of water. Then, 1.2 mL of freshly-made 0.10 M $NaBH_4$(aq) was quickly injected to the above mixture and stirred vigorously for 2 h. Then, the prepared seed solution was aged for at least one week. The growth solution was prepared by adding 5.0 mL of acetonitrile(l), 75 μL of 0.10 M L-ascorbic acid(aq) and 0.20 mL of 75 mM TSC(aq) into 10 mL of water in an ice bath. In the growth solution, silver ions were reduced by L-ascorbic acid(aq), a weak reducing agent, that allows for silver seeds to grow slowly into well-defined AgPRs [31-33]. Under vigorous stirring, 12 mL of the aged silver seed solution was added to the growth solution, followed by addition of 60 μL of 0.10 M $AgNO_3$(aq) to initiate the growth of silver seeds. After stirring for 5 min, the reaction mixture was aged without disturbance for additional 55 min to produce Ag-PRs. AuAg-PRs were prepared by drop-wisely adding 0.15 mL of 0.10 mM $HAuCl_4$(aq) into 2.5 mL of the above Ag-PR colloid, which was then stirred for 15 min. The products, where the intended molar ratio of Au to Ag was 0.023, were

centrifuged and washed with water at 9,000 rpm for 10 min and dispersed in 0.16 mL of water.

Synthesis of P3HT@AuAg-PRs. The detailed preparation and characterization of P3HT-SH having M_n of 10,565 g mol^{-1} have already been reported [20,34]. P3HT@AuAg-PRs were synthesized under ambient conditions as described in detail elsewhere [35] with little modifications. First, 0.13 mL of concentrated 0.25 g L^{-1} P3HT-SH in THF was added to 40 μL of the AuAg-PR colloid. The intended molar ratio of P3HT-SH to Ag was calculated to be 55 in this case. Then, the mixed colloid was sonicated for 10 min and undisturbed for at least 24 h in the dark. As-prepared P3HT@AuAg-PRs were centrifuged and washed twice with THF at 12,000 rpm for 10 min and redispersed in 0.30 mL of THF. For the synthesis of P3HT-grafted silver nanoprisms (P3HT@Ag-PRs), the Ag-PR colloid was used instead of the AuAg-PR colloid with the same procedure.

Characterization. Transmission electron microscopy (TEM) images were obtained with a H-7600 Hitachi microscopy while high-resolution TEM (HRTEM) and scanning TEM (STEM) images, as well as energy-dispersive X-ray (EDX) elemental maps and profiles, were measured using a JEOL JEM-2100F microscope. X-ray photoelectron spectroscopy (XPS) spectra, as well as static and time-resolved spectra of absorption and emission, were obtained as reported [34]. For the SERS measurement of P3HT@AuAg-PRs, a quartz plate (0.5 cm x 0.5 cm) was washed with acetone three times and dried under N_2(g). Then, 10 μL of P3HT@AuAg-PRs dispersed in THF was dropped on the quartz plate and dried at least for 5 min for complete solvent evaporation. This process was repeated for three additional times. SERS spectra were measured with excitation at 532 nm by using an OLYMBUS BX41 confocal microscope Raman system having a SLOC Laser GL532RA-100 DPSS laser. Each SERS spectrum was

averaged over four measurements. The stability of each colloid in the presence of 0.82 mM H_2O_2(aq) was measured by monitoring absorption spectral changes at scheduled intervals.

1.4. Results and Discussion

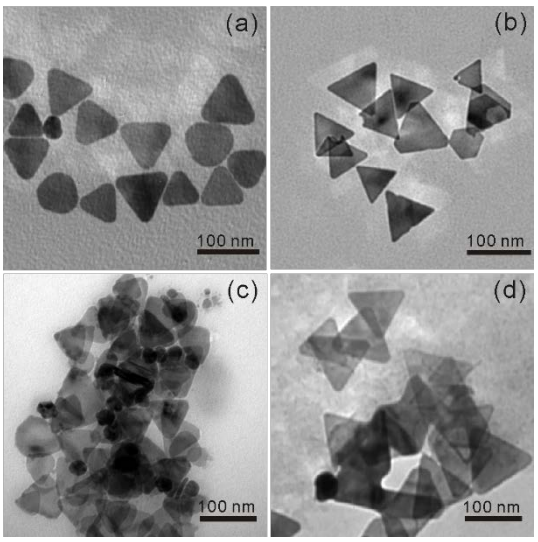

Figure 1-2. TEM images of (a) Ag-PRs, (b) AuAg-PRs, (c) P3HT@Ag-PRs, and (d) P3HT@AuAg-PRs.

As-prepared P3HT@AuAg-PRs were facilely fabricated by blending P3HT-SH in THF with AuAg-PRs dispersed in water and these nanocomposites were further investigated for their optical properties and stability in the colloidal state. Figure 1-2a,b and Figure 1-S1 show that the sharp tips of AuAg-PRs with an average edge length of 122 ± 10 nm having a typical thickness of ~8 nm were maintained in water whereas the tips of Ag-PRs became rounded with an average edge length of 79 ± 10 nm. According to a previous report [29], introduced $HAuCl_4$ would induce the galvanic replacement with silver atoms preferentially around the edges of Ag-PR. The relative surface energies associated with the crystallographic planes of a face-

centered cubic silver are in the order of $\gamma_{110} > \gamma_{100} > \gamma_{111}$ and gold atoms initially replace the silver atoms at the edges which are mainly represented by (110) and (100) planes [7]. Subsequently, the silver/gold alloyed structure at the edges of Ag-PR would start to form due to their close lattice-spacing values [7]; the incorporated gold would make a great contribution to stabilize the sharp tips of Ag-PR. The TEM images of Figure 1-2c,d show that the sizes of Ag-PRs and AgAu-PRs have been hardly changed after grafting P3HT chains on the surfaces of nanoprisms. However, the TEM images of Figure 1-2c,d also demonstrate that the tip rounding of P3HT@Ag-PRs has taken place to a certain degree in THF whereas the sharp tips of P3HT@AuAg-PRs have been still maintained.

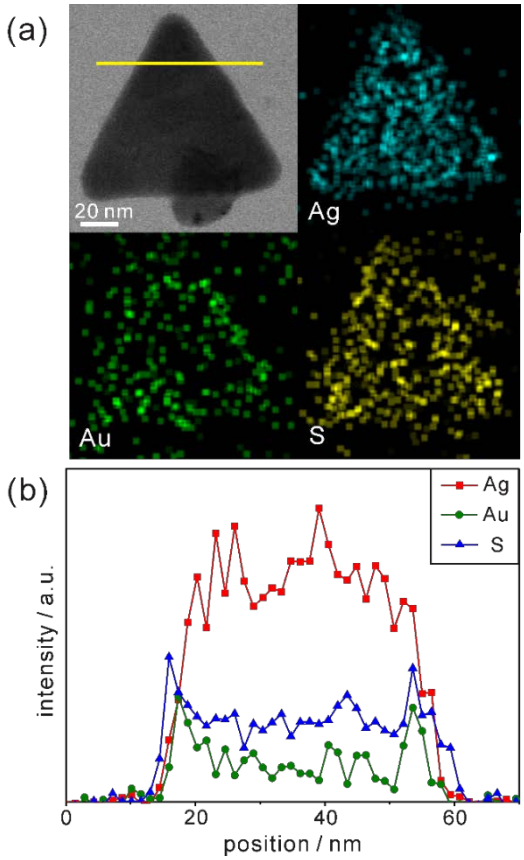

Figure 1-3. (a) STEM image and EDX maps of P3HT@AuAg-PR. (b) EDX profiles of P3HT@AuAg-PR.

Furthermore, line-scanned EDX elemental profiles as well as EDX elemental maps have been measured to confirm the exact structure and compositions of P3HT@AgAu-PR (Figure 1-3). The STEM image and EDX elemental maps of Figure 1-3a reveal that sulfur atoms, which represent the presence of P3HT chains, exist on the surface of AuAg-PR with a full coverage while gold atoms are epitaxially coating the edges of Ag-PR with a frame-like structure. The EDX elemental profiles of Figure 1-3b indicate that silver atoms have gathered as a solid structure whereas gold or sulfur atoms, having two characteristic peaks, are present in a hollow or shell structure. Figure 1-3b has also revealed that the line-scanned edge lengths of silver, gold, and sulfur are 38, 42, and 45 nm, respectively. Based on these observations, we suggest that Ag-PR is epitaxially coated with gold atoms and that P3HT chains cover AuAg-PR fully, making P3HT@AuAg-PRs miscible with organic solvents such as THF. The EDX analysis spectrum of Figure 1-S2 provides the specific molar percentages of silver, gold, and sulfur as 88.8%, 8.7%, and 2.5%, respectively. Considering this and the average size of Ag-PRs, we have calculated that 4.4×10^3 P3HT chains surround one AuAg-PR, meaning that the molar mass of P3HT@AuAg-PR is 4.7×10^7 g mol^{-1}. Then, the weight ratio of P3HT chains to AuAg-PRs can be calculated as 0.14 because the molar masses of AuAg-PR and P3HT have been found to be 3.3×10^8 g mol^{-1} and 1.1×10^4, respectively.

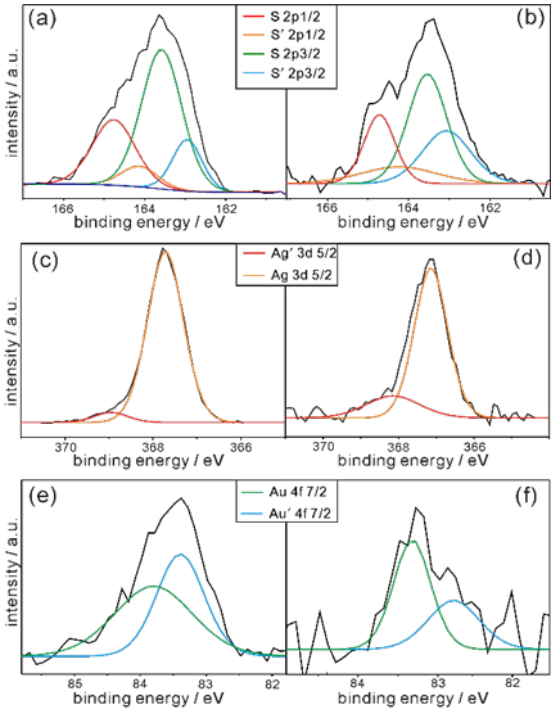

Figure 1-4. XPS spectra of (a) pristine P3HT-SH, (b,d,f) P3HT@AuAg-PRs, and (c,e) AuAg-PRs for sulfur (top), silver (middle), and gold (bottom).

The XPS data of Figure 1-4 can provide further significant information on chemical bonds between the surfaces of AuAg-PR and the thiol groups of P3HT. The S 2p XPS spectrum of pristine P3HT in Figure 1-4a has been resolved via curve deconvolution into two sets of doublet peaks having a splitting of 1.18 eV and an area ratio of 1:2 in agreement with the value from the theoretical spin-orbit effect (Table 1-S1). These two sets of peaks account for two types of sulfur species in pristine P3HT; a set of S $2p_{1/2}$ and S $2p_{3/2}$ corresponds to thiophene rings while the other set of S´ $2p_{1/2}$ and S´ $2p_{3/2}$ corresponds to free terminal thiol groups. As shown in Table 1-S1, the peak positions of the S species of P3HT@AuAg-PRs are quite similar to those of pristine P3HT, supporting that sulfur atoms in the thiophene rings of P3HT chains have hardly been affected by forming nanocomposites with AuAg-PRs. However, the peak positions of S´ species of P3HT@AuAg-PRs are shifted to higher binding energies by 0.12 eV than those

of P3HT-SH, providing an evidence that free terminal thiol groups are interacting with the surfaces of nanoprisms. In particular, the positive shifts of the binding energies suggest that the sulfur atoms of the terminal thiol groups of P3HT chains are mostly attached to gold because the electronegativity of gold (2.54) is higher than that of the hydrogen atom (2.20). Note that the electronegativity of silver (1.93) is even smaller than that of the hydrogen atom. This also supports that the surfaces of Ag-PRs have been well-coated with gold and most P3HT-SH chains bind chemically with gold. The abundance percentage of the S´ species of P3HT@AuAg-PRs related to free terminal thiol groups is 16.3% higher than that of pristine P3HT-SH, also demonstrating that the terminal thiol groups of P3HT molecules are chemically bound to the surfaces of AuAg-PRs [36].

The individual Ag 3d and Au 4f XPS spectra of P3HT@AuAg-PRs and AuAg-PRs in Figure 1-4 have also been deconvoluted into doublet peaks (Table 1-S2), suggesting that gold atoms as well as silver atoms have two different environments. In case of silver, the binding energy of Ag´ $3d_{5/2}$ is higher than that of Ag $3d_{5/2}$ because Ag´ atoms are neighboring with gold atoms rather than other silver atoms. Note that the electronegativity of silver is lower than that of gold as we mentioned. This is also supported from the fact that the abundance percentage of Ag´ $3d_{5/2}$ (5.2%) is much smaller than that of Ag $3d_{5/2}$ (94.8%) because only a small amount of silver atoms are interacting with gold atoms on the edges of nanoprisms. On the other hand, the gold atoms of Au´ $4f_{7/2}$ with a lower binding energy represent that they are neighboring with silver atoms because of the aforementioned reason. Figure 1-4 and Table 1-S2 also indicate that the XPS spectra of both Ag 3d and Au 4f in P3HT@AuAg-PRs have been shifted from the respective ones in AuAg-PRs, also supporting that the thiol terminal groups of P3HT molecules interact chemically with the surfaces of nanoprisms.

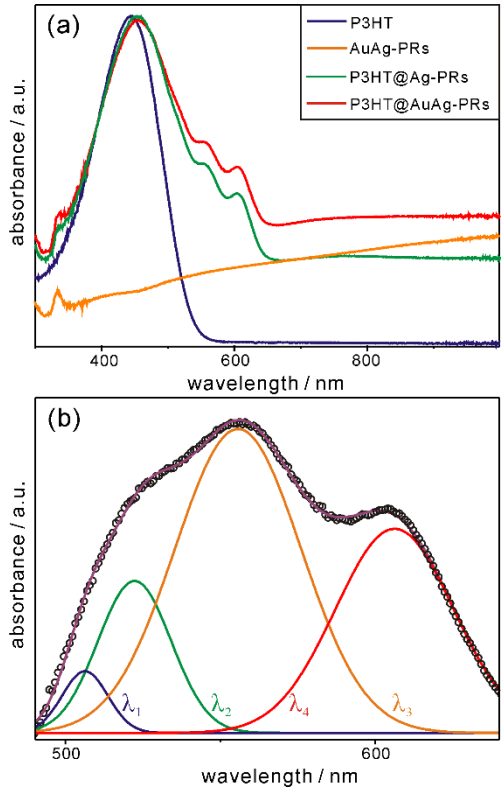

Figure 1-5. (a) Absorption spectra of P3HT, AuAg-PRs, P3HT@Ag-PRs, and P3HT@AgAu-PRs dispersed in THF. (b) Absorption difference spectrum from 490 nm to 640 nm (circles) obtained by subtracting the absorption spectra of pristine P3HT and AuAg-PRs from the absorption spectrum of P3HT@AuAg-PRs in (a), fitted with Gaussian curves of λ_1, λ_2, λ_3, and λ_4.

Figure 1-5a shows that each absorption spectrum of pristine P3HT, P3HT@Ag-PRs, and P3HT@AuAg-PRs in THF contains a broad band at 450 nm due to the characteristic intrachain π-π transition of P3HT chains. In addition, each absorption spectrum of P3HT@Ag-PRs and P3HT@AuAg-PRs contains two characteristic bands at 556 and 606 nm. It has been reported that when a poly(3-alkylthiophene) is mixed with a poor solvent, the absorption bands in the range of 490-610 nm appear due to energy hopping between neighboring chains [37]. Since the solvent of P3HT@Ag-PRs or P3HT@AuAg-PRs is the same as the solvent of pristine P3HT, the advent of these two bands can be assigned to P3HT interchain aggregates, resulting from the grafting of P3HT-SH chains on the surfaces of noble-metal nanoprisms. The absorption

spectrum of Ag-PRs dispersed in water (Figure 1-S3) exhibits peaks at 331, 544, and 804 nm corresponding to the out-of-plane quadrupole, in-plane quadrupole, and in-plane dipole modes, respectively, of surface-plasmon resonances (SPRs) [19]. A red shift by 18 nm of the dipole mode with 3 nm broadening has been observed after the incorporation of gold to Ag-PRs, indicating the galvanic replacement of silver with gold. The in-plane dipole modes of P3HT@Ag-PRs and P3HT@AuAg-PRs in THF have been observed as broad featureless bands. It is noteworthy that the absolute absorption strength of P3HT@AuAg-PRs in Figure 1-5a is much less pronounced than that of AuAg-PRs in Figure 1-S3 due to the high density of grafted P3HT on the surfaces of the nanoprisms.

For more profound observation on chemical interactions between the thiol groups of P3HT-SH and the surfaces of nanoprisms, we have attained the absorption difference spectrum by subtracting the absorption spectra of pristine P3HT and AuAg-PRs from the absorption spectrum of P3HT@AuAg-PRs (Figure 1-5b). The appearance of absorption peaks from 470 nm to 650 nm has been assigned to P3HT aggregates having strong interchain and intrachain interactions [38]. Figure 1-5b and Table 1-S3 show that the subtracted absorption spectrum can be deconvoluted into four curves of λ_1, λ_2, λ_3, and λ_4 having the maxima at 506, 522, 556, and 606 nm, respectively. According to a previous report [34], the λ_1 curve originates from amorphous chains whereas the λ_2, λ_3, and λ_4 curves correspond to the 0-2, 0-1, and 0-0 transitions of aggregated P3HT molecules, respectively. Thus, this also supports that the thiol terminal groups of P3HT molecules bind chemically to the surfaces of nanoprisms, making P3HT@AuAg-PRs stable and miscible with THF.

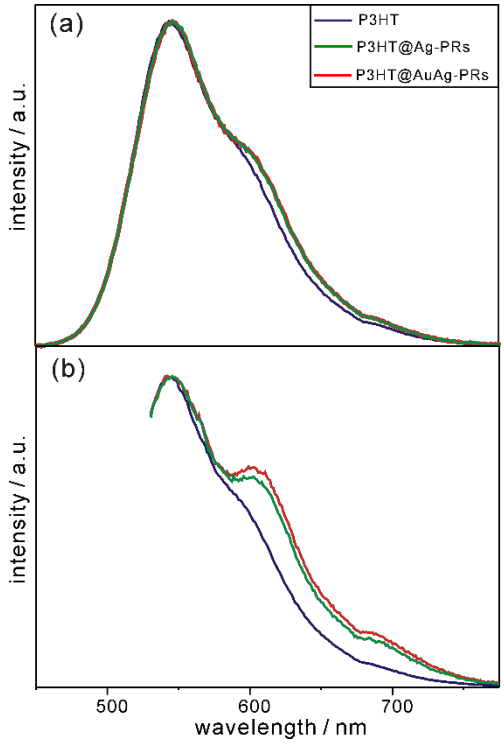

Figure 1-6. Fluorescence spectra of pristine P3HT, P3HT@Ag-PRs, and P3HT@AuAg-PRs in THF, after excitation at (a) 355 nm and (b) 532 nm.

As shown in Figure 1-6, each emission spectrum of pristine P3HT, P3HT@Ag-PRs, and P3HT@AuAg-PRs contains three main parts: the peak around 550 nm ascribed to the 0-0 transition of free P3HT chains originating from the recombination of S_1 excitons to the ground state, a shoulder around 620 nm, and a tail around 690 nm. The shoulder and the tail are attributed to transitions from the S_1 state to the lowest vibrational level of the ground state (0-0) and the first-excited vibrational level of the ground state (0-1), respectively, of aggregated P3HT chains [39]. Particularly, both the shoulder and the tail of P3HT@Ag-PRs and P3HT@AuAg-PRs are stronger than the respective ones of pristine P3HT, supporting that the thiol groups of P3HT are bound on the surfaces of nanoprisms, inducing for P3HT chains to be aggregated as described in Figure 1-1. Note that the shoulder as well as the tail in the emission spectra of P3HT@Ag-PRs and P3HT@AuAg-PRs is much more prominent with excitation of

532 nm than with excitation of 355 nm because aggregated P3HT molecules are excited more efficiently by photons with a lower energy [39]. This also supports that P3HT chains are compactly surrounding the surfaces of noble-metal nanoprisms, as presented in Figure 1-1. In addition, the shoulder and the tail of P3HT@AuAg-PRs are more protrudent than the respective ones of P3HT@Ag-PRs. This implies that the thiol groups of P3HT molecules bind more strongly with gold surfaces than silver surfaces [40], making P3HT@AuAg-PRs more stable than P3HT@Ag-PRs (see below).

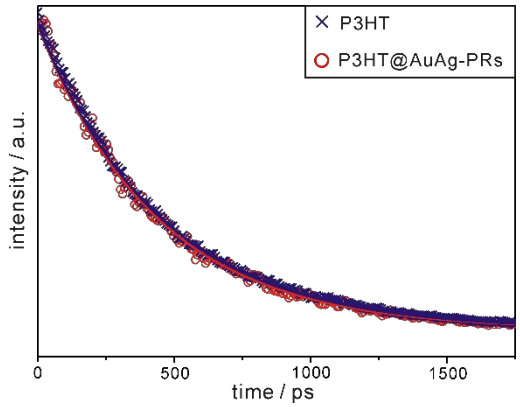

Figure 1-7. Picosecond emission decay profiles of P3HT and P3HT@AuAg-PRs in THF. Samples have been excited with 355 nm pulses and probed at 580 nm, and solid lines indicate best-fitted curves.

We have obtained the fluorescence and transient-absorption decay profiles of pristine P3HT and P3HT@AuAg-PRs in THF to understand photophysical interactions between excitons of P3HT and SPRs of AuAg-PRs. Figure 1-7 shows that the picosecond emission decay kinetic profiles can be fitted into a single component, which arises from the relaxation of S_1 excitons, of 450 ps for pristine P3HT and 437 ps for P3HT@AuAg-PRs (Table 1-1). In a previous paper [20], the relaxation time of S_1 excitons in P3HT-coated gold nanoparticles has been found to be shorter than that in pristine P3HT owing to energy transfer from P3HT to gold nanoparticles.

Accordingly, the shorter decay time of P3HT@AuAg-PRs demonstrates that energy transfer to the SPR states of AuAg-PRs reduces the relaxation time of S_1 excitons in P3HT to some extent through chemical bonds between the thiol terminal groups of P3HT molecules and the noble-metal surfaces of AuAg-PRs.

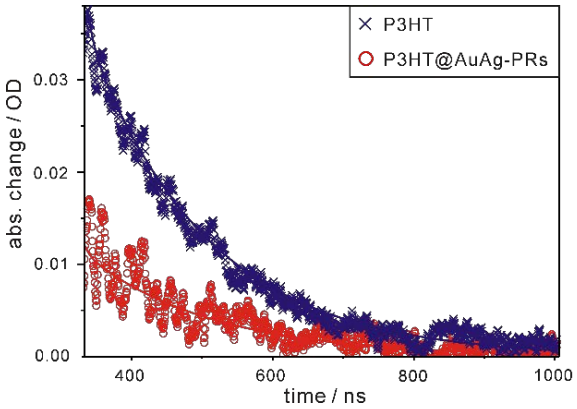

Figure 1-8. Nanosecond transient-absorption decay profiles of P3HT and P3HT@AuAg-PRs in THF. Samples have been excited at 355 nm and probed at 820 nm, and solid lines show best-fitted curves.

Table 1-1. Fluorescence and transient-absorption decay constants of P3HT and P3HT@AuAg-PRs in THF.

Method	Sample	Decay time (ps)
Picosecond emission[a]	P3HT	450
	P3HT@AuAg-PR	437
Nanosecond absorption[b]	P3HT	170,000
	P3HT@AuAg-PR	180,000

[a]Excited at 355 nm and collected at 580 nm. [b]Excited at 355 nm and monitored at 820 nm

Likewise, each nanosecond transient-absorption decay profile of pristine P3HT and P3HT@AuAg-PRs dispersed in THF (Figure 1-8) has been fitted into a single component of 170 ns for P3HT and 180 ns for P3HT@AuAg-PRs (Table 1-1), showing the lifetime of T_1 excitons. The amplitude of T_1 absorption in P3HT@AuAg-PRs is less than that in pristine

P3HT, revealing that T_1 excitons in P3HT@AuAg-PRs are less populated due to the inefficient intersystem crossing of S_1 excitons into the T_1 state. On the contrary to the obtained decay times of S_1 exitons, T_1 excitons in P3HT@AuAg-PRs decay slightly slower than those in pristine P3HT because aggregated P3HT chains bound on the surfaces of AuAg-PRs have rigid and stretched conformations [31]. Considering the reduced amplitude and the increased decay time of T_1 excitons in P3HT@AuAg-PRs, we assert that neither the intersystem crossing of S_1 into T_1 nor the intersystem crossing of T_1 into S_0 takes place effectively in P3HT@AuAg-PRs owing to the high rigidity of aggregated P3HT chains.

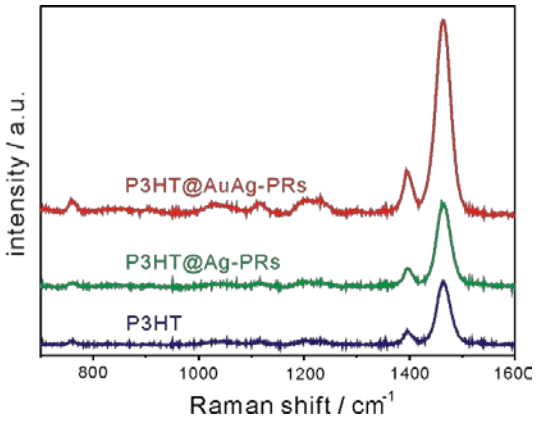

Figure 1-9. Raman spectra of pristine P3HT, P3HT@Ag-PRs, and P3HT@AuAg-PRs. The concentration of P3HT was fixed and all the samples were excited at 532 nm.

As shown in Figure 1-9, the Raman signals of pristine P3HT, P3HT@Ag-PRs, and P3HT@AuAg-PRs have been measured to examine the SERS effect of nanoprisms. Previous approaches to the fabrication of a thin film with Ag-PRs have typically required the surface functionalization of a glass substrate with 3-aminopropyltrialkoxysilane and the subsequent adhesion of Ag-PRs; these processes are time-consuming and difficult to control [18,28]. On the other hand, our each Raman sample has been prepared by just dropping a colloid on a quartz slide since the surfaces of nanoprisms have already been functionalized with P3HT. Under 532

nm excitation which can resonant with the SPR absorption of nanoprisms, the enhancement of Raman scattering has been observed for both P3HT@Ag-PRs and P3HT@AuAg-PRs. The Raman intensity at 1464 cm^{-1}, which arises from the in-phase stretching of the C=C thiophene ring, of P3HT@Ag-PRs is higher by a factor of 1.5 than that of pristine P3HT due to the typical SERS effect of Ag-PRs [18]. It has been reported that the sharp corners of silver nanoprisms have relatively high field so that enhanced plasmonic electric field would be generated within the gap between silver nanoprisms, enhancing SERS effect [7]. The Raman intensity of P3HT@AuAg-PRs is even 3.1 times higher than that of P3HT@Ag-PRs because the sharp tips of AuAg-PRs generate higher field enhancement than edge-rounded Ag-PRs do, as expected from the lightning-rod effect. Thus, the protected sharp tips of AuAg-PRs act as "hot spots" to enhance SERS effect as high as 4.6 (Figure 1-S4).

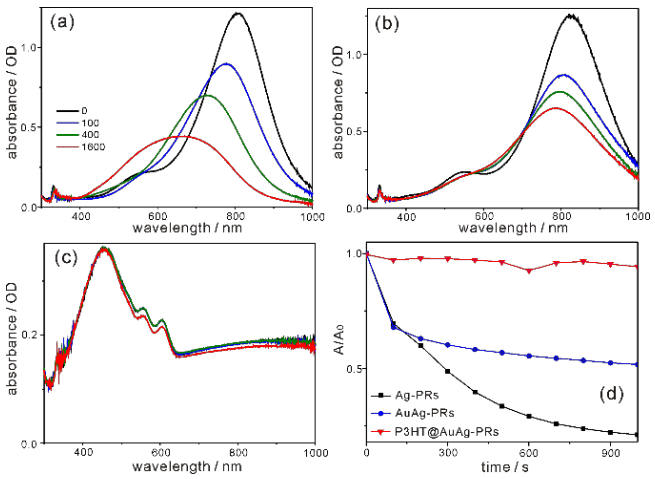

Figure 1-10. Absorption spectral evolutions of (a) Ag-PRs and (b) AuAg-PRs dispersed in water and (c) P3HT@AuAg-PRs dispersed in THF after treatment with H_2O_2. (d) A/A_0 vs *t* at 804 nm for Ag-PRs, 823 nm for AuAg-PRs, and 998 nm for P3HT@AuAg-PRs.

Figure 1-10a,b shows that the SPR absorption of Ag-PRs has been blue-shifted enormously by 134 nm whereas that of AuAg-PRs is blue-shifted by a small degree of 33 nm after treatment

with H_2O_2. This demonstrates that gold coating on the edges of Ag-PRs has brought about structurally highly stable AuAg-PRs. Typically, gold coating on the surfaces of silver nanoparticles enhances structural stability because, compared with silver, gold is much more inert to oxidation [13,30]. Figure 1-10c shows that the absorption of P3HT@AuAg-PRs in the range of 650-1000 nm, which arises from the SPR dipole mode of AuAg-PRs, has remained almost invariant after treatment with H_2O_2. It is noteworthy that P3HT@AuAg-PRs is even more stable than AuAg-PRs because P3HT chains act as a stabilizer, enhancing the structural stability extensively. To obtain a profound insight into the morphology deformation of nanoprisms over time, the absorption changes of nanoprisms after treatment with H_2O_2 have been fitted to the first-order kinetics; $\ln (A / A_0) = - k t$, where k is the deformation rate constant of nanoprisms, t is the monitored time, and A (A_0) is the SPR absorbance of nanoprisms at the time t (0). It is a pivotal point that the half lifetime ($t_{1/2} = \ln 2 \ k^{-1}$) for the morphology deformation of P3HT@AuAg-PRs (290 min) has been extended 48 and 22 times longer than the half lifetimes of Ag-PRs (6 min) and AuAg-PRs (13 min), respectively (Table 1-S4). This suggests that the structural stability of Ag-PRs can be enhanced by gold coating on the edges of Ag-PRs, leading to AuAg-PRs whose stability can be further improved extensively by the protection of aggregated P3HT chains on the surfaces of AuAg-PRs. Thus, it has been shown that the edge gold coating and the subsequent thiol-functionalized P3HT grafting of Ag-PRs have enhanced not only optical properties but also feasible-process ability. Furthermore, the resultant P3HT@AuAg-PRs have enormously high stability against oxidizing agents, extending the use of noble-metal nanoprisms for various optical applications.

1.5. Conclusions

Silver nanoprisms (Ag-PRs) have been expitaxially edge-coated with gold atoms and subsequently covered fully with poly(3-hexylthiophene) (P3HT) chains, leading to poly(3-hexylthiophene-grafted edge-gold-coated silver nanoprisms (P3HT@AuAg-PRs) which are miscible well with organic solvents; individual AuAg-PRs with an average edge length of 122 nm and a typical thickness of 8 nm have been surrounded by 4.4 x 10^3 P3HT chains. In fluorescence spectra, a shoulder at 620 nm is much stronger in P3HT@AuAg-PRs than in pristine P3HT, designating that the thiol groups of P3HT molecules compactly surround the surfaces of nanoprisms. In addition, picosecond emission kinetic profiles suggest that the S_1 relaxation time of P3HT in P3HT@AuAg-PRs is reduced due to energy transfer from P3HT to AuAg-PRs. From nanosecond transient-absorption kinetic profiles, the reduced amplitude and the increased decay time of T_1 excitons in P3HT@AuAg-PRs have been measured, indicating that neither the intersystem crossing of S_1 into T_1 nor the intersystem crossing of T_1 into S_0 occurs effectively in P3HT@AuAg-PRs owing to the stretched and rigid conformations of P3HT chains bound on the surfaces of AuAg-PRs. The SERS effect of P3HT@AuAg-PRs is as high as 4.6 because the sharp tips of AuAg-PRs which are maintained via gold coating serve as “hot spots”. The half lifetime for the morphology deformation of P3HT@AuAg-PRs in H_2O_2(aq) has been extended 48 times longer than that of Ag-PRs. Overall, our fabricated P3HT@AuAg-PRs have not only feasible-process ability but also enhanced optical properties. Furthermore, the nanocomposites possess high stability against oxidizing agents, extending the use of noble-metal nanoprisms for various optical applications.

1.6. Acknowledgments

This work was financially supported by research grants from the National Research Foundation of Korea (2015-051798 and 2014-057382).

1.7. Supporting Information

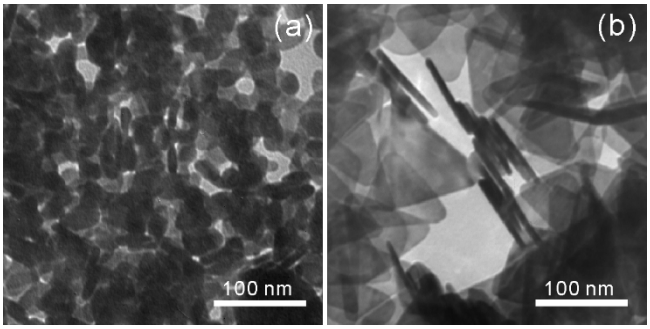

Figure 1-S1. TEM images of (a) Ag-PRs and (b) AuAg-PRs.

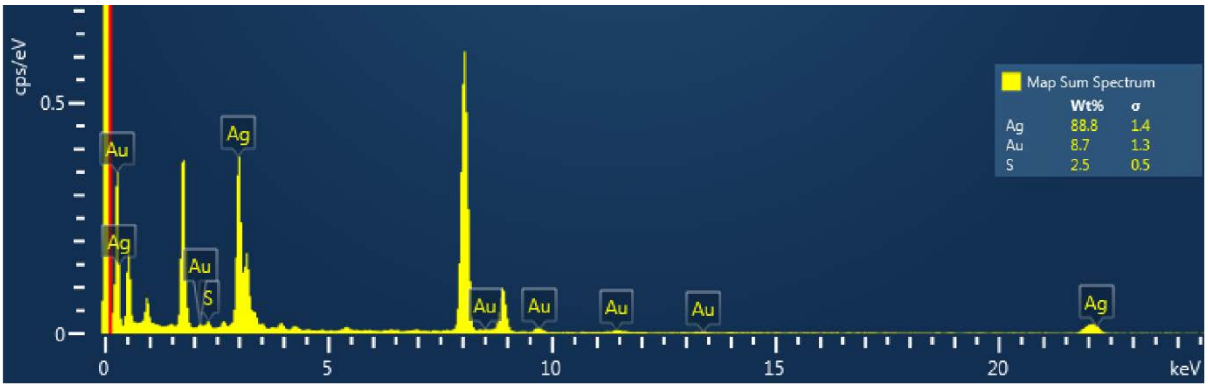

Figure 1-S2. EDX analysis spectrum of P3HT@AuAg-PRs, where the molar percentages of silver, gold, and sulfur have been observed to be 88.8%, 8.7%, and 2.5%, respectively.

Table 1-S1 Binding energies in eV for the deconvoluted curves of S 2p XPS spectra.

Sample	S $2p_{1/2}$	S $2p_{3/2}$	S´ $2p_{1/2}$	S´ $2p_{3/2}$
P3HT	164.76 (26.3%)	163.58 (52.5%)	164.13 (7.1%)	162.95 (14.1%)
P3HT@AuAg-PR	164.72 (20.8%)	163.54 (41.7%)	164.25 (12.5%)	163.07 (25.0%)

Table 1-S2 Binding energies in eV for the deconvoluted curves of Ag 3d and Au 4f XPS spectra.

Sample	Ag´ $3d_{5/2}$	Ag $3d_{5/2}$	Au $4f_{7/2}$	Au´ $4f_{7/2}$
AuAg-PR	368.95 (5.2%)	367.72 (94.8%)	83.80 (52.6%)	83.39 (47.4%)
P3HT@AuAg-PR	368.15 (19.3%)	367.14 (80.7%)	83.32 (61.9%)	82.80 (38.1%)

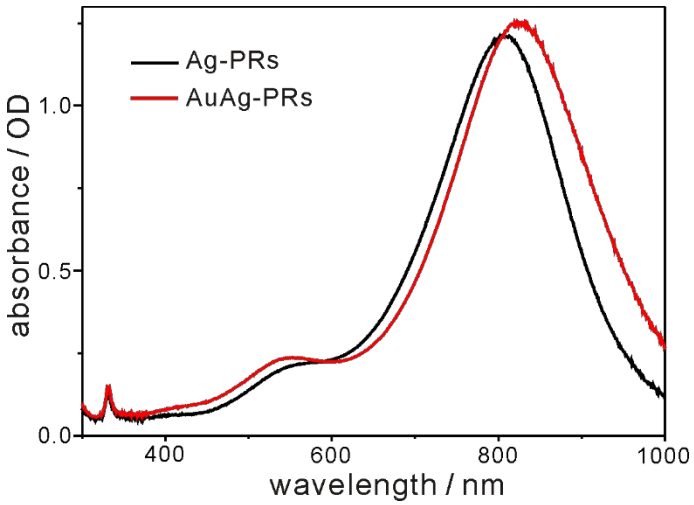

Figure 1-S3. Absorption spectra of Ag-PRs and AuAg-PRs dispersed in water.

Table 1-S3. Spectral positions of four Gaussian curves extracted from the subtracted absorption spectrum of Figure 5b.

λ_1 / nm	λ_2 / nm	λ_3 / nm	λ_4 / nm
506±9 (4%)[a]	522±14 (14%)	556±26 (50%)	606±22 (32%)

[a]Absorbance percentage of each curve.

Table 1-S4. Half lifetimes ($t_{1/2}$) for the morphology deformation of nanoprisms via H_2O_2.

Samples	$t_{1/2}$ / min
Ag-PR	6
AuAg-PR	13
P3HT@AuAg-PR	290

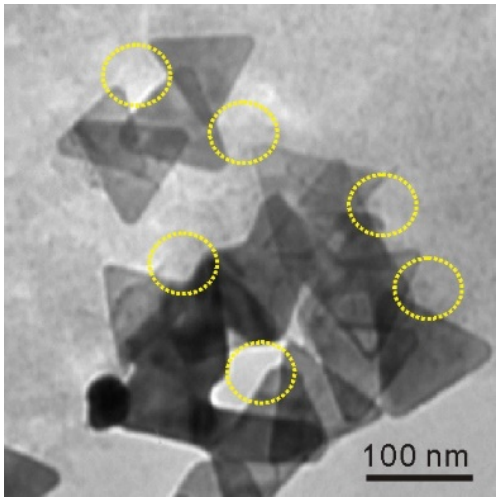

Figure 1-S4. TEM image of P3HT@AuAg-PRs and hot spots marked with yellow-dotted circles.

1.8. References

[1] B. Jana, S. Bhattacharyya and A. Patra, *Phys. Chem. Chem. Phys.*, 2015, **17**, 15392-15399.

[2] J. Lee and D.-J. Jang, *J. Phys. Chem. C*, 2016, **120**, 4130-4138.

[3] J. Lee and D.-J. Jang, *RSC Adv.*, 2015, **5**, 64268-64273.

[4] M. A. Mahmoud, *Langmuir*, 2013, **29**, 6253-6261.

[5] H. A. Atwater and A. Polman, *Nat. Mater.*, 2010, **9**, 205-213.

[6] E. Martinsson, M. M. Shahjamali, K. Enander, F. Boey, C. Xue, D. Aili and B. Liedberg, *J. Phys. Chem. C*, 2013, **117**, 23148-23154.

[7] J. Sun, X. Wang, J. Liu, P. Wan, Q. Liao, F. Wang, L. Luo and X. Sun, *RSC Adv.*, 2014, **4**, 35263-35267.

[8] C. Gao, Z. Lu, Y. Liu, Q. Zhang, M. Chi, Q. Cheng and Y. Yin, *Angew. Chem. Int. Edit.*, 2012, **51**, 5629-5633.

[9] Q. Zhang, J. Ge, T. Pham, J. Goebl, Y. Hu, Z. Lu and Y. Yin, *Angew. Chem. Int. Edit.*, 2009, **121**, 3568-3571.

[10] Q. Zhang, N. Li, J. Goebl, Z. Lu and Y. Yin, *J. Am. Chem. Soc.*, 2011, **133**, 18931-18939.

[11] Y. Gu, S. Kong, X. Diao, Y. Guo, K. Zhang and H. He, *New J. Chem.*, 2016, **40**, 7557-7563.

[12] M. Stavytska-Barba, M. Salvador, A. Kulkarni, D. S. Ginger and A. M. Kelley, *J. Phys. Chem. C*, 2011, **115**, 20788-20794.

[13] D. Aherne, D. E. Charles, M. E. Brennan-Fournet, J. M. Kelly and Y. K. Gun'ko, *Langmuir*, 2009, **25**, 10165-10173.

[14] M. -S. Hsu, Y. -W. Cao, H. -W. Wang, Y. -S. Pan, B. -H. Lee and C. -L. Huang, *Chemphyschem*, 2010, **11**, 1742-1748.

[15] B. Marta, E. Jakab, M. Potara, T. Simon, F. Imre-Lucaci, L. Barbu-Tudoran, O. Popescu and S. Astilean, *Colloids Surf. A Physicochem. Eng. Asp.*, 2014, **441**, 77-83.

[16] P. Du, P. Jing, D. Li, Y. Cao, Z. Liu and Z. Sun, *Small*, 2015, **11**, 2454-2462.

[17] C. Xue, X. Chen, S. J. Hurst and C. A. Mirkin, *Adv. Mater.*, 2007, **19**, 4071-4074.

[18] L. Liu and T. L. Kelly, *Langmuir*, 2013, **29**, 7052-7060.

[19] B.-H. Lee, M.-S. Hsu, Y.-C. Hsu, C.-W. Lo and C.-L. Huang, *J. Phys. Chem. C*, 2010, **114**, 6222-6227.

[20] D. Lee and D.-J. Jang, *Polymer*, 2014, **55**, 5469-5476.

[21] F. Monnaie, W. Brullot, T. Verbiest, J. De Winter, P. Gerbaux, A. Smeets and G. Koeckelberghs, *Macromolecules*, 2013, **46**, 8500-8508.

[22] R. C. Advincula, *Dalton Trans.*, 2006, 2778-2784.

[23] E. Stratakis and E. Kymakis, *Mater. Today*, 2013, **16**, 133-146.

[24] L. Lu, Z. Luo, T. Xu and L. Yu, *Nano Lett.*, 2012, **13**, 59-64.

[25] D. H. Wang, D. Y. Kim, K. W. Choi, J. H. Seo, S. H. Im, J. H. Park, O O. Park and A. J. Heeger, *Angew. Chem. Int. Edit.*, 2011, **123**, 5633-5637.

[26] S. Kazim, J. Pfleger, M. Procházka, D. Bondarev and J. Vohlídal, *J. Colloid Interf. Sci.*, 2011, **354**, 611-619.

[27] L. Scudiero, H. Wei and H. Eilers, *ACS Appl. Mater. Inter.*, 2009, **1**, 2721-2728.

[28] A. P. Kulkarni, K. M. Noone, K. Munechika, S. R. Guyer and D. S. Ginger, *Nano Lett.*, 2010, **10**, 1501-1505.

[29] M. M. Shahjamali, M. Salvador, M. Bosman, D. S. Ginger and C. Xue, *J. Phys. Chem. C*, 2014, **118**, 12459-12468.

[30] X. Liu, L. Li, Y. Yang, Y. Yin and C. Gao, *Nanoscale*, 2014, **6**, 4513-4516.

[31] N. R. Jana, T. K. Sau and T. Pal, *J. Phys. Chem. B*, 1999, **103**, 115-121.

[32] K. Mallik, M. Mandal, N. Pradhan and T. Pal, *Nano Lett.*, 2001, **1**, 319-322.

[33] N. R. Janafi, Z. L. Wangl and T. K. Sau, *Curr. Sci.*, 2000, **79**, 1367-1369.

[34] D. Lee, S. Jeong, J.-H. Park, S. Y. Park and D.-J. Jang, *J. Mater. Sci.*, 2016, **51**, 9669-9678.

[35] Z. Nie, D. Fava, E. Kumacheva, S. Zou, G. C. Walker and M. Rubinstein, *Nat. Mater.*, 2007, **6**,

609-614.

[36] M. Turner, O. P. H. Vaughan, G. Kyriakou, D. J. Watson, L. J. Scherer, G. J. E. Davidson, J. K. M. Sanders and R. M. Lambert, *J. Am. Chem. Soc.*, 2009, **131**, 1910-1914.

[37] M. He, L. Zhao, J. Wang, W. Han, Y. Yang, F. Qiu and Z. Lin, *ACS nano*, 2010, **4**, 3241-3247.

[38] B. Ferreira, P. F. da Silva, J. S. S. de Melo, J. Pina and A. Macanita, *J. Phys. Chem. B*, 2012, **116**, 2347-2355.

[39] D. Lee, J. K. Kim and D.-J. Jang, *Polymer*, 2016, **99**, 122-129.

[40] H. Sellers, A. Ulman, Y. Shnidman and J. E. Eilers, *J. Am. Chem. Soc.*, 1993, **115**, 9389-9401.

Chapter 2. One-Step Polypyrrole Coating of Self-Assembled Silver Nanoprisms for Enhanced Stability and Raman Scattering

2.1. Abstract

Self-assemblies of silver nanoprisms (AgPRs) having enhanced structural stability and optical properties have been facilely coated with polypyrrole (PPy) *via* the *in situ* polymerization of pyrrole monomers that also act as an assembling agent. The assemblies of AgPRs, whose edge lengths and thicknesses are typically 78 and 6 nm, respectively, have been surrounded by PPy coating of 6 nm. AgPRs are assembled in an edge-to-edge orientation, and the degree of assembly has been controlled by varying the concentration of trisodium citrate dihydrate, which attaches selectively to the {111} facets of AgPRs. The morphology deformation time of PPy-coated AgPRs in 0.6 mM H_2O_2(aq) is 7 times longer than that of PPy-free AgPRs, suggesting that PPy coating prevents the sharp tips of AgPRs from being truncated by oxidizing agents. The SERS effect of highly self-assembled and PPy-coated AgPRs becomes as high as 6.3 due to numerous hot spots generated between nanoprisms. Overall, our fabricated AgPRs assemblies with PPy coating have not only improved structural stability but also enhanced optical properties, extending the practical use of noble-metal nanoprisms for various optical applications.

2.2. Introduction

The design and fabrication of noble-metal nanoparticles have received immense attention for catalysis, optoelectronics, surface-enhanced Raman scattering (SERS), and biosensing due to their unique optical properties, originating from their compositions, sizes, and shapes [1-4]. Recently, many studies have been focused on controlling the assembly of noble-metal nanoparticles for SERS applications due to their interesting optical and structural properties which cannot be found from individual nanoparticles [5-7]. In general, the driving forces of the assembly are chemical-bonding and hydrogen-bonding interactions, electrostatic forces, van der Waals interactions, or combinations of these forces between nanoparticles [8]. Particularly, facet-selective ligand adsorption on the surfaces of nanoparticles has been introduced to allow facile control over the degree of self-assembly [9]. The crystal facet-selective ligand adsorption has been applied to induce the assembly of aniostropic nanoparticles such as nanorods and nanoprisms due to their interesting size- and shape-dependent properties [8]. However, it has been a challenge to achieve control over the assembly by the facet-selective functionalization of anisotropic nanostructures. To now, a number of researches have explored the facet-selective assembly of nanorods [10-12]. For example, Fava et al. have reported that the preferential binding of cetyltrimethyl ammonium bromide (CTAB) and polystyrene molecules on the sides and ends, respectively, of gold nanorods allows to control over the end-to-end or side-to-side assembly of gold nanorods depending on solvents [10]. Nie et al. have considered the aforementioned assembly structure of a gold nanorod as a triblock copolymer since their side is covered with a bilayer of hydrophilic CTAB while their end facets are covered with hydrophobic polymers [11,12]. Yet, the assembly of nanoprisms arising from facet-selective ligand adsorption has rarely been studied because the edges of nanoprisms, where atoms are

highly active, are unstable and susceptible to truncation when they are exposed to solvents or assembling ligands [13].

Silver nanoprisms (AgPRs) have been widely investigated for applications such as solar cells, catalysts, and sensors due to massive electromagnetic field enhancement and high sensitivity, which are attributed to the sharp tips of AgPRs [14-17]. For example, Barba et al. have reported that the intensity of the Raman spectra of organic materials on a substrate covered with AgPRs is extensively enhanced due to a high electromagnetic field generated by the sharp tips of AgPRs [18]. The assembly of AgPRs can amplify the electromagnetic field within the gap between nanoprisms. Geng et al. have demonstrated that the Raman intensity of probe molecules on the AgPRs substrate can be enhanced owing to the tendency of close packing, generating hot spots between AgPRs [19]. Xue et al. have mentioned that the enhanced Raman intensity of 4-mercaptobenzoic acid is due to the highly ordered and large-scaled self-assembly of AgPRs consisting of six-tip-based hot spots generated by a slow drying process on a silicon wafer [20]. However, these approaches of AgPR assemblies have required a solvent evaporation process. Although the assembly of AgPRs in a colloidal state has been studied by using DNA as an assembling agent [21], yet, it has been a challenge to control the side-to-side or face-to-face assemblies of AgPRs in a colloidal state.

Typically, the assembly of noble-metal nanoparticles in solvents is prone to disassembly because the linker molecules can be dissolved into solvents, resulting in irregular aggregation of nanoparticles [22]. Thus, protective coating surrounding the assembled nanoparticles is essential to improve stability for practical applications, especially, in a colloidal system. A number of papers have introduced silica coating to protect assembled nanostructures [23,34]. Recently, polypyrrole (PPy) coating has also been considered because it is biocompatible and requires a simple coating procedure [25]. PPy coating has often been incorporated to enhance

the stability of the assembled nanostructures against external factors such as air, water, and organic solvents [26,27]. In fact, the adsorption of pyrrole (Py) monomers, which are electrolytes, on the surfaces of metal nanoparticles can also induce metal nanoparticles to assemble by reducing electrostatic repulsion forces between nanoparticles prior to polymerization [22].

Herein, we are reporting a one-step polypyrrole (PPy) coating process of self-assembled silver nanoprisms (AgPRs) through the direct polymerization of pyrrole (Py) monomers that also act as an assembling agent by using silver ions as a mild oxidizing agent (Figure 2-1). The *in situ* polymerization of Py monomers that surround self-assembled AgPRs has enhanced structural stability against oxidizing agents and in organic solvents. We have observed that AgPRs tend to be assembled in an edge-to-edge orientation by pyrrole molecules and the degree of assembly has been controlled by varying the amount of trisodium citrate dihydrate (TSC), which attaches selectively on the faces of AgPRs. PPy-coated self-assembled AgPRs have shown extended morphology-deformation time and enhanced SERS effect, broadening the practical usability of noble-metal nanoprisms for various optical applications.

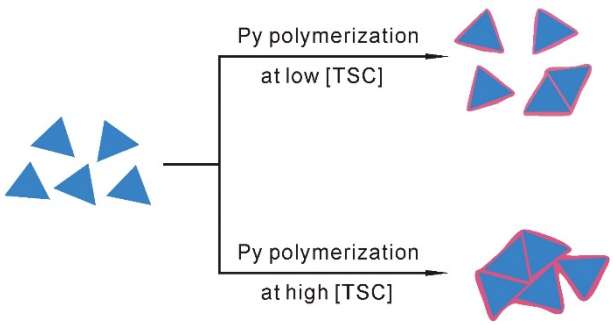

Figure 2-1. Schematically presented PPy coating of self-assembled AgPRs on the surfaces of AgPRs, depending on the concentration of TSC. Blue and red colors represent silver and PPy, respectively.

2.3. Experimental Section

Chemicals. Chemicals were used as received: silver nitrate ($AgNO_3$, s, ≥99%), trisodium citrate dihydrate (TSC, $Na_3C_6H_5O_7$, s, ≥99%), L-ascorbic acid (s, ≥99%), and sodium borohydride ($NaBH_4$, s, ≥99%), pyrrole (Py, C_4H_5N, l, ≥98%), 4-mercaptobenzoic acid (4MBA, $HSC_6H_4CO_2H$, s, ≥99%), and iron(III) chloride hexahydrate ($FeCl_3 \cdot 6H_2O$, s, ≥97%) from Sigma-Aldrich; acetonitrile (l, ≥99%) from Ducksan Pharmaceutical; sodium hydroxide (NaOH, s, ≥99%) from EMSURE; H_2O_2 (aq, 34%) from Samchun Pure Chemicals. Ultrapure deionized water (>15 MΩ cm) from an Elga PURELAB option-S system was used throughout the experiments.

Synthesis of AgPRs and pristine PPy. AgPRs were synthesized by a seed-mediated growth method [28]. The seed solution was prepared by adding 12 mL of 75 mM TSC(aq), 0.20 mL of 0.10 M $AgNO_3$(aq), and 0.42 mL of 34% H_2O_2(aq) in 200 mL of water. Then, 1.2 mL of 0.10 M $NaBH_4$(aq) was added to the above mixture and stirred for 2 h. The prepared seed solution was aged for one week prior to use. The growth solution was prepared by adding 5.0 mL of acetonitrile(l), 75 μL of 0.10 M L-ascorbic acid(aq), and 0.20 mL of 75 mM TSC(aq) into 10 mL of water in an ice bath; in the growth solution, L-ascorbic acid(aq) was used as a weak reducing agent for silver seeds to grow slowly into AgPRs [29-31]. Under stirring, 12 mL of the seed solution was added to the growth solution, followed by the addition of 60 μL of 0.10 M $AgNO_3$(aq). The reaction mixture was aged for 1 h to produce AgPRs. The 24 mL of the reaction mixture was collected to centrifuge at 9000 rpm for 10 min and dispersed in 0.76 mL of water.

The pristine PPy was prepared by adding 50 μL of Py(l) to 10 mL of 0.16 M $FeCl_3$(aq) in

an ice bath [32]. After being aged for 18 h, the mixture was washed with water three times at 8000 rpm for 5 min and collected for characterization.

Synthesis of PPy-coating of self-assembled AgPRs. The self-assembly of AgPRs was induced by diluting 16 μL of the above AgPRs colloid, a specified volume of 75 mM TSC(aq), and 0.50 mL of 0.36 M Py(l) to 2.0 mL using water; the added volumes of TSC(aq) were 0, 5, 10, 50, and 100 μL for samples AgPRs/TSC-0, AgPRs/TSC-5, AgPRs/TSC-10, AgPRs/TSC-50, and AgPRs/TSC-100, respectively. Then, the silver ions, which were ionized from the surfaces of AgPRs, acted as a mild oxidizing agent, initiating the polymerization of Py to produce PPy [33,34]. After being aged for 2 days, PPy-coated self-assembled AgPRs were collected and washed with water 3 times at 13000 rpm for 5 min and dispersed in 0.20 mL of water.

Characterization. Transmission electron microscopy (TEM) images were obtained with a H-7600 Hitachi microscopy. Absorption spectra were measured using a UV/vis spectrophotometer (Scinco, S-3100) while Fourier transform infrared (FT-IR) spectra were obtained using a Bruker Vertex80v FTIR spectrometer with KBr pressed disks. For the SERS measurement of PPy-coated self-assembled AgPRs, a glass substrate was washed with acetone and dried under N_2(g) and then, 10 μL of each sample dispersed in water was dropped on the glass substrate and dried under ambient conditions. 10 μL of an aqueous solution containing 50 mM 4MBA and 0.2 M of NaOH was dropped on each substrate [19]. SERS spectra were measured with excitation at 532 nm by using an OLYMBUS BX41 confocal microscope Raman system with a SLOC Laser GL532RA-100 DPSS laser. Note that each SERS spectrum was obtained by averaging over three measurements at different spots. The stability of each

colloid in the presence of 0.61 mM H_2O_2(aq) was tested by monitoring absorption spectral changes at scheduled intervals.

2.4. Results and Discussion

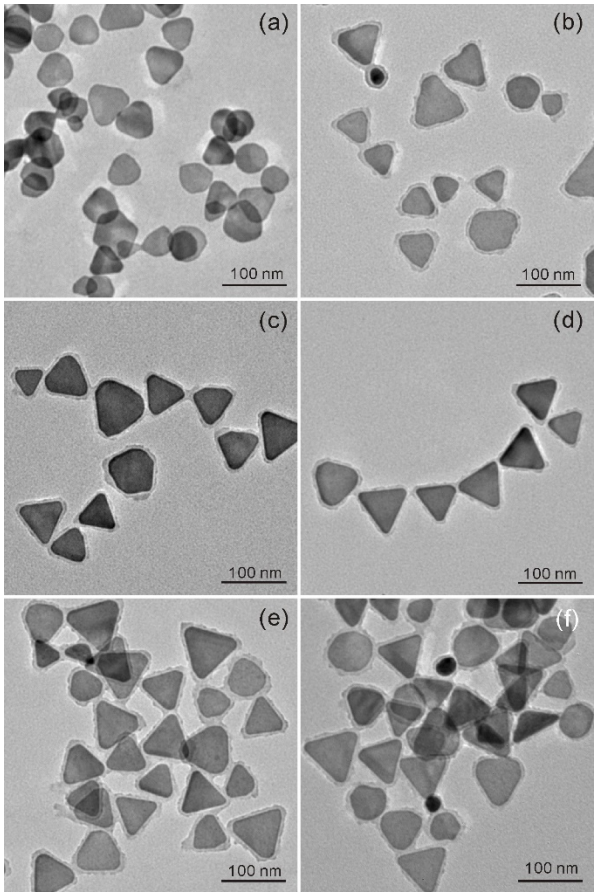

Figure 2-2. High-resolution TEM images for (a) PPy-free AgPRs and PPy-coated AgPRs of (b) AgPRs/TSC-0, (c) AgPRs/TSC-5, (d) AgPRs/TSC-10, (e) AgPRs/TSC-50, and (f) AgPRs/TSC-100.

Figure 2-2 exhibits that the sharp tips of PPy-coated AgPRs with an average edge length of 78 ± 9 nm having a typical thickness of ~4 nm were well-maintained by PPy coating of ~6 nm whereas the tips of PPy-free AgPRs were truncated over the aging period in water to have an

average edge length of 54 ± 8 nm with a thickness of ~9 nm. This indicates that PPy coating has well prevented AgPRs from exposure to solvents, bringing about the enhanced stability of nanoprism tips. In Figure 2-2 and Figure 2-1S, as the concentration of TSC during the assembling period increases, the majority of AgPRs tend to assemble well in a side-to-side orientation. Note that PPy-free AgPRs have been loaded with random orientations on a TEM grid, because the morphology of nanoparticles in a colloidal state changed inevitably during a solvent drying process, resulting in aggregation, reorganization, or dissociation [22]. The self-assembly degree of AgPRs depending on the concentration of TSC was further investigated by counting the numbers of assembled AgPRs from TEM images (Figure 2-S1). PPy-coated AgPRs have been mainly observed as monomers or dimers at a low concentration of TSC whereas more than 70 AgPRs have been assembled together and surrounded by PPy coating at a high concentration of TSC. The statistical number percentage of AgPRs in assemblies with more than 70 nanoprisms has been calculated to be 90% (Figure 2-S1e), revealing that the concentration of TSC is a key factor determining the degree of AgPR assemblies. Note that AgPRs tend to assemble in a side-to-side orientation, indicating that Py molecules would attach mainly to the sides of AgPRs prior to polymerization to produce PPy (see below).

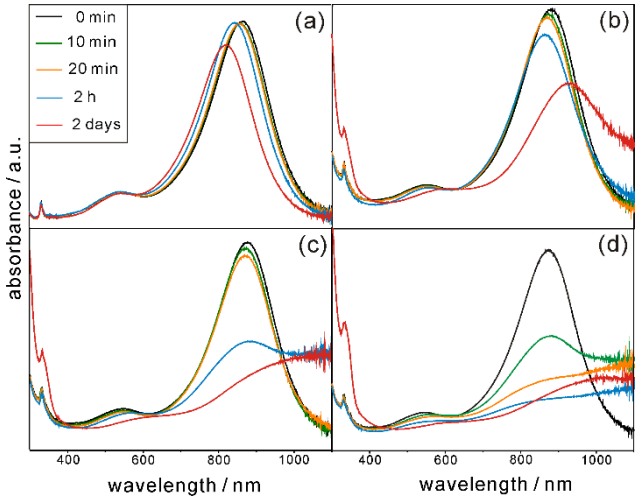

Figure 2-3. Absorption spectra of (a) AgPRs in the absence of Py and (b) AgPRs/TSC-0, (c) AgPRs/TSC-10, and (d) AgPRs/TSC-100 in the presence of Py, recorded as a function of time after diluting AgPRs colloids in water.

Figure 2-3 shows that the surface-plasmon resonance (SPR) band of TSC-capped AgPRs in the absence of Py has been blue-shifted by 10 nm in 20 min while that of AgPRs/TSC-10 in the presence of Py molecules has been blue-shifted by 5 nm. It has been discussed that the SPR absorption of AgPRs can be blue-shifted when the vertices of AgPRs get truncated by water, organic solvents, oxidizing agents, or other harsh conditions [13]. This indicates that the vertices of TSC-capped AgPRs without Py molecules have been truncated since TSC molecules, which bind selectively to the faces of AgPRs, hardly prevent the sides of AgPRs from being oxidized, while the sharp tips of AgPRs can be stabilized to some extent by the adsorption of Py molecules on the sides of AgPRs, leading to a smaller blue shift [35]. Meanwhile, in particular, Figure 2-3d shows that a new band around 1000 nm arises in 20 min in the absorption spectra of AgPRs/TSC-100 with Py molecules due to a SPR coupling of highly assembled AgPRs. Note that the Py molecules have acted as an assembling agent. After aging for 2 h, the SPR band of TSC-capped AgPRs without Py has been further blue-shifted

by 23 nm whereas that of AgPRs/TSC-10 in the presence of Py has been red-shifted by 5 nm; furthermore, that of AgPRs/TSC-100 has been extremely red-shifted by 211 nm with an isobetic point at 963 nm, indicating a side-to-side orientation of AgPRs. Thus, we suggest that the concentration of TSC is a key factor for controlling the degree of AgPR assemblies at a fixed Py concentration.

It has been well-known that TSC binds selectively with the {111} facets of AgPRs, which are the top and bottom faces of AgPRs [35]. So, as the concentration of TSC gets higher in a AgPRs colloid, the {111} facets of AgPRs would be covered more densely with TSC molecules, preventing other molecules from being attached on the faces of AgPRs. Meanwhile, the adsorption of Py molecules to the surfaces of AgPRs induces the self-assembly of AgPRs; according to a previous report [22], Py monomers adsorb on surfaces of nanoparticles and greatly lower interparticle electrostatic repulsion forces, inducing the assembly of nanoparticles. Thus, a possible assembly mechanism can be postulated from Figure 2-2 and Figure 2-3; when the faces of AgPRs are fully covered with TSC molecules, Py molecules would prefer to attach on the sides of AgPRs, inducing the side-to-side assembly of AgPRs. Then, the self-assembled AgPRs have been aged for 2 days to allow the *in situ* polymerization of Py to form PPy.

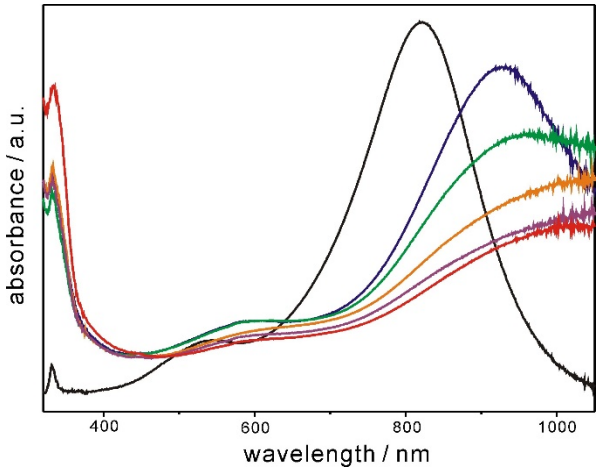

Figure 2-4. Absorption spectra of (black) PPy-free AgPRs and PPy-coated AgPRs of (blue) AgPRs/TSC-0, (green) AgPRs/TSC-5, (orange) AgPRs/TSC-10, (purple) AgPRs/TSC-50, and (red) AgPRs/TSC-100 dispersed in water.

Figure 2-4 shows that the absorption spectrum of PPy-free AgPRs exhibits peaks at 331, 545, and 804 nm, which arise from the out-of-plane quadrupole, in-plane quadrupole, and in-plane dipole modes, respectively, of SPRs, while each absorption spectrum of PPy-coated AgPRs colloids shows an additional SPR band beyond 900 nm due to the assembly of AgPRs. It is noteworthy that the additional SPR band of PPy-coated AgPRs tends to be red-shifted further upon increase of the TSC concentration, indicating that AgPRs have assembled together to a higher degree. In addition, the absorbance peak at 331 nm for PPy-coated AgPRs is more pronounced compared with that for PPy-free AgPRs, due to the absorption band arising from the π-π* transition of PPy chains [35]. Thus, we consider that Py molecules, which were bound to the surfaces of AgPRs, have been polymerized to form PPy by using silver ions as a mild oxidizing agent. This supports that the assembly degree of AgPRs can be controlled by varying the concentration of TSC and that the *in situ* polymerization of Py occurs to produce PPy shells, making PPy-coated AgPRs stable and well-miscible with organic solvents.

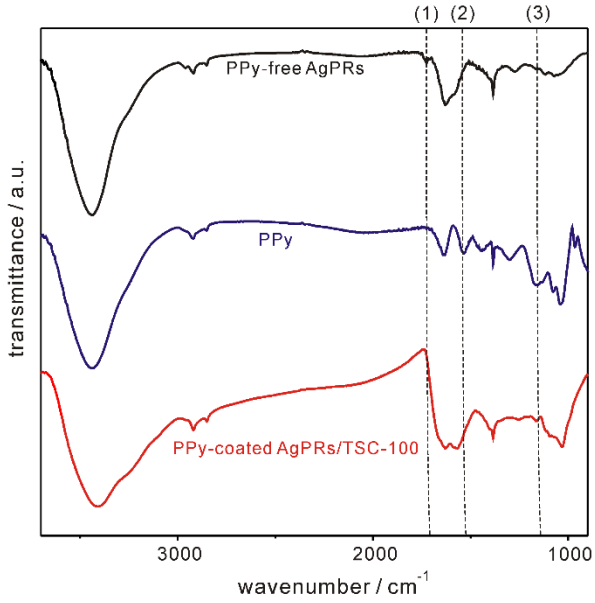

Figure 2-5. FTIR spectra of PPy-free AgPRs, pristine PPy, and PPy-coated AgPRs/TSC-100: (1) C=O stretching at 1726 cm^{-1}, (2) N–H bending at 1536 cm^{-1}, and (3) C–N stretching at 1164 cm^{-1}.

The FTIR spectra in Figure 2-5 also support that Py molecules attached to the surfaces of AgPRs have been polymerized to form PPy, surrounding self-assembled AgPRs. The FTIR peak from the C=O stretching mode of AgPRs at 1726 cm^{-1} supports the presence of TSC molecules. This agrees well with the FTIR spectrum of TSC-capped silver nanoparticles in a previous report [34]. Note that the C=O stretching peaks of both pristine PPy and PPy-coated AgPRs/TSC-100 have disappeared, indicating that TSC molecules on the surfaces of AgPRs have been replaced completely by Py molecules. The FTIR pattern of PPy-coated AgPRs/TSC-100 from 1000 to 1500 cm^{-1} resembles that of pristine PPy due to their inherently existing pyrrole rings having N-H bending and C-N stretching modes [38,39]. Thus, we declare that the polymeric shells surrounding AgPRs observed from the TEM images in Figure 2-2 and Figure 2-S1 have been facilely fabricated by the *in situ* polymerization of Py without introducing any additional oxidizing agent, enhancing the structural stability of self-assembled AgPRs extensively (see below).

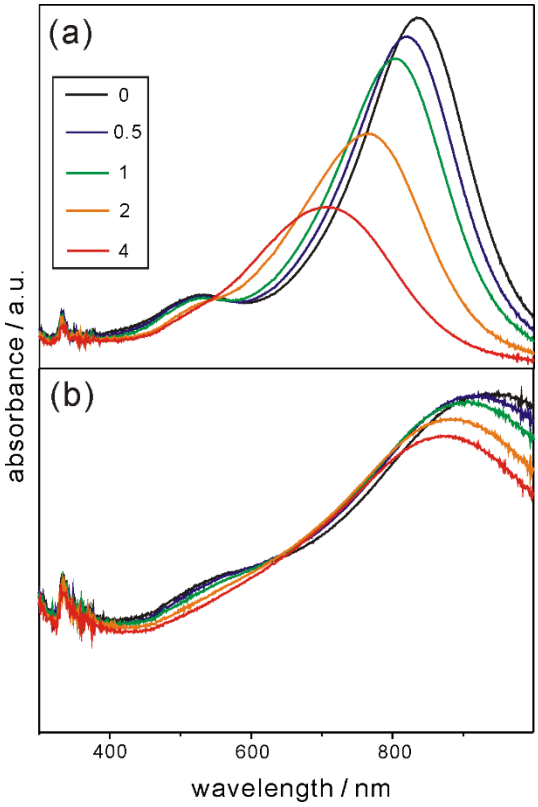

Figure 2-6. Absorption spectral evolutions of (a) PPy-free AgPRs and (b) PPy-coated AgPRs/TSC-100 after treatment with H_2O_2(aq) for periods indicated in the units of min.

Figure 2-6 shows that the SPR band of PPy-free AgPRs has been extensively shifted to the blue by 129 nm whereas that of PPy-coated AgPRs/TSC-100 has been shifted to the blue by only 56 nm after treatment with H_2O_2(aq). This observation shows that PPy coating has brought about the improved structural stability of AgPRs. It has been reported that PPy coating enhances the structural stability and reusability of noble-metal nanoparticles for catalysts [26]. Note that as PPy-coated AgPRs/TSC-100, used for stability test, was aged for 2 days, their AgPRs have been covered with thin PPy shells of ~6 nm in thickness. As shown in Figure 2-S2, the thickness of a PPy shell can be further increased simply by aging for a longer period. Since Py molecules can also act as stabilizers to preserve the morphology of AgPRs well, a sample aged for a specific period was dispersed in ethanol to monitor the formation of PPy

shells clearly. Figure 2-S2a shows that when a AgPRs colloid containing Py was aged for just one day and dispersed in ethanol, the tips of nanoprisms were enormously truncated into disk-like structures. This indicates that the aging time of one day is not long enough for nanoprisms to be covered with sufficiently thick PPy shells. Meanwhile, from Figure 2-S2b-d, the thickness values of PPy shells have been measured to be 6, 7, and 17 nm after aging for 2, 3, and 7 days, respectively, indicating that the morphologies of AgPRs have been maintained well in ethanol. This supports that PPy coating enhances indeed the morphological stability of AgPRs in organic solvents. We consider that thicker PPy coating would bring about even higher structural stability of AgPRs against oxidizing agents as well as organic solvents.

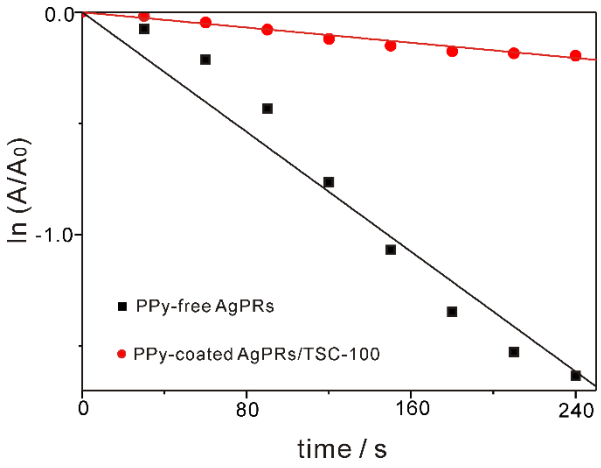

Figure 2-7. ln(A/A_0) vs *t* after treatment with H_2O_2(aq), monitored at 833 nm for PPy-free AgPRs and 935 nm for PPy-coated AgPRs/TSC-100.

To gain a profound insight on the morphology deformation of nanoprisms over time, the absorption evolutions of nanoprisms after treatment with H_2O_2(aq) have been considered as the first-order kinetics [3]; $\ln (A / A_0) = - k t$, where k is the deformation rate constant of nanoprisms, t is the observed time, and A (A_0) is the SPR band absorption of nanoprisms at time t (0). It is crucial that the half lifetime ($t_{1/2} = \ln 2\ k^{-1}$) for the morphology-deformation of PPy-coated

AgPRs/TSC-100 (14 min) has been extended 7 times longer than the half lifetime of PPy-free AgPRs (2 min), suggesting that the stability of AgPRs can be extensively improved even with thin PPy coating of ~6 nm. Figure 2-S2 and Figure 2-S3 show that AgPRs without properly thick PPy coating suffer instant morphology deformation rapidly in ethanol whereas self-assembled AgPRs with sufficient PPy coating are highly stable. Thus, we can suggest that PPy coating enhances the structural stability of nanoprisms greatly against strong oxidants and organic solvents.

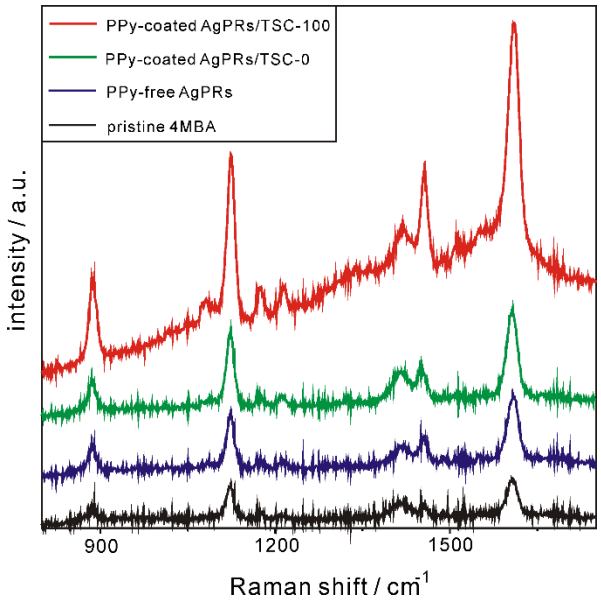

Figure 2-8. Raman spectra of 4MBA on (black) glass, (blue) PPy-free AgPRs, (green) PPy-coated AgPRs/TSC-0, and (red) PPy-coated AgPRs/TSC-100 substrates with excitation at 532 nm.

The SERS performances of self-assembled AgPRs have been measured using 4MBA as a reporter molecule. As shown in Figure 2-8, the Raman signals of individual samples exhibit two intense peaks at 1060 and 1595 cm^{-1}, which are attributed to the characteristic aromatic ring-breathing modes of 4MBA [19]. Under 532 nm excitation, the Raman intensity at 1595 cm^{-1} of PPy-free AgPRs is larger by a factor of 1.9 than that of pristine 4MBA owing to the

typical SERS performance of silver nanoparticles [40]. Meanwhile, the Raman intensity of PPy-coated AgPRs/TSC-0 is 2.4 times bigger than that of pristine 4MBA due to the sharp tips of AgPRs maintained well by PPy coating. Furthermore, the Raman intensity of PPy-coated AgPRs/TSC-100 is even 6.3 times larger than that of pristine 4MBA because highly self-assembled AgPRs with near-field coupling would generate numerous hot spots between neighboring nanoprisms. Thus, it has been shown that a high degree of self-assemblies enhances SERS effect enormously while the *in situ* PPy coating of assembled AgPRs increases structural stability greatly against oxidizing agents or organic solvents, broadening the use of nanoprisms for various optical applications.

2.5. Conclusions

Self-assemblies of silver nanoprisms (AgPRs) having enhanced stability and optical properties have been facilely coated with polypyrrole (PPy) *via* the *in situ* polymerization of pyrrole (Py) monomers that also act as an assembling agent; the assemblies of AgPRs, whose edge lengths and thicknesses are typically 78 and 6 nm, respectively, have been surrounded by PPy coating of 6 nm. PPy-coated AgPRs have been mainly observed as monomers or dimers at a low concentration of trisodium citrate dihydrate (TSC), which attaches selectively to the {111} facets of AgPRs. At a high concentration of TSC, more than 70 AgPRs have been assembled together and surrounded by PPy coating; the faces of AgPRs are fully covered with TSC molecules, leading to the adsorption of Py molecules mainly on the sides of AgPRs. Furthermore, the increased red shift of surface-plasmon resonances beyond 900 nm upon increase of the TSC concentration has suggested that the assembly degree of AgPRs can be

controlled by varying the concentration of TSC. The half lifetime for the morphology deformation of PPy-coated AgPRs in H_2O_2(aq) has been extended 7 times longer than that of PPy-free AgPRs, suggesting that PPy coating prevents the sharp tips of AgPRs from being truncated by oxidizing agents. The SERS effect of highly self-assembled and PPy-coated AgPRs is as high as 6.3 due to numerous hot spots generated between nanoprisms. Overall, our one-step PPy-coating of self-assembled AgPRs enhances not only structural stability but also optical properties, broadening the practical use of noble-metal nanoprisms for various optical applications.

2.6. Acknowledgement

This work was financially supported by a research grant from the National Research Foundation of Korea (2015-051798).

2.7. Supporting information

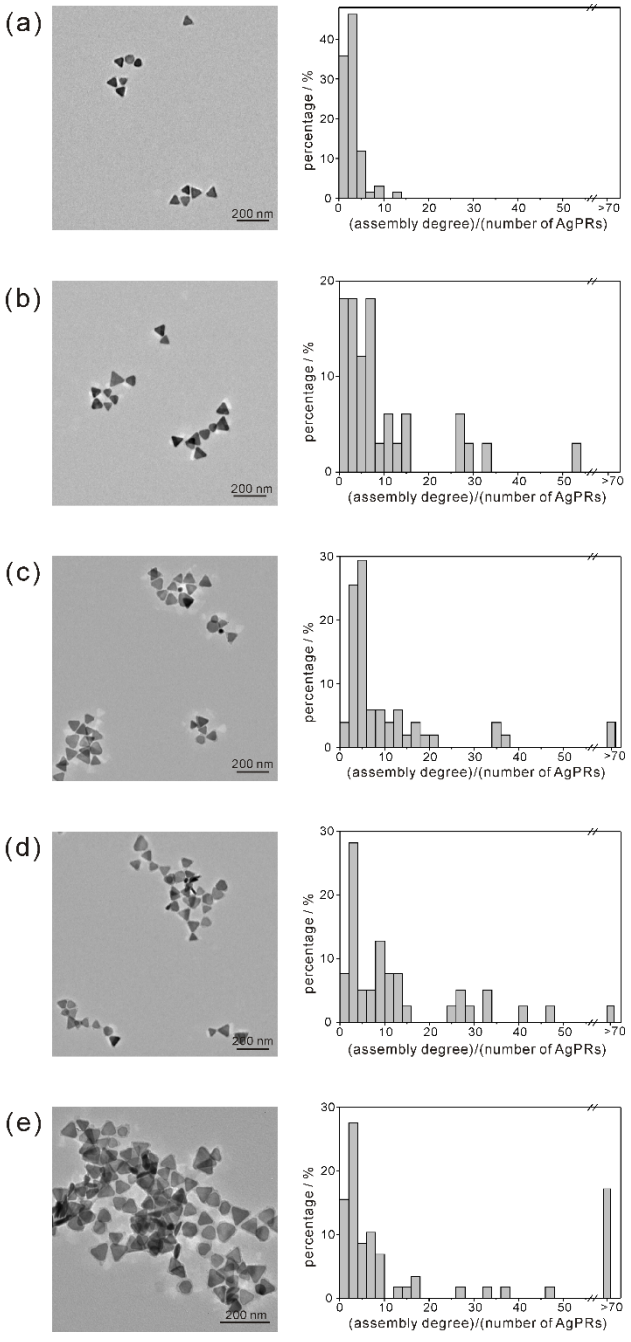

Figure 2-S1. Low-resolution TEM images (left) and assembly-degree histograms (right) of (a) AgPRs/TSC-0, (b) AgPRs/TSC-5, (c) AgPRs/TSC-10, (d) AgPRs/TSC-50, and (e) AgPRs/TSC-100.

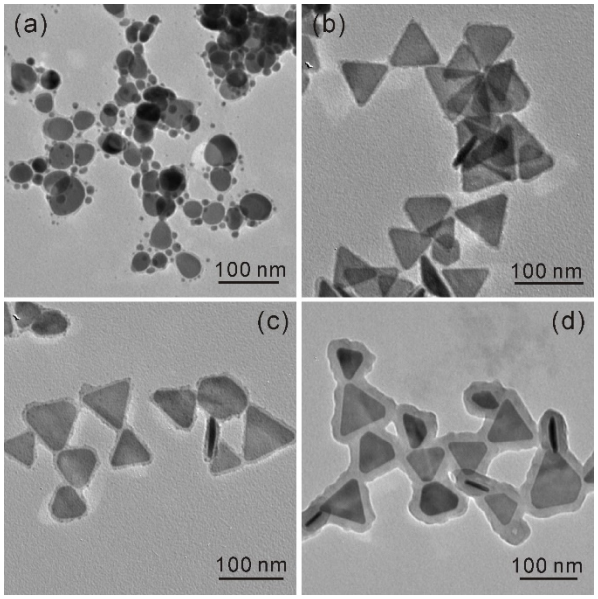

Figure 2-S2. TEM images of AgPRs/TSC-100 aged for (a) 1, (b) 2, (c) 3, and (d) 7 days in the presence of Py. Note that each sample was dispersed in ethanol prior to TEM loading.

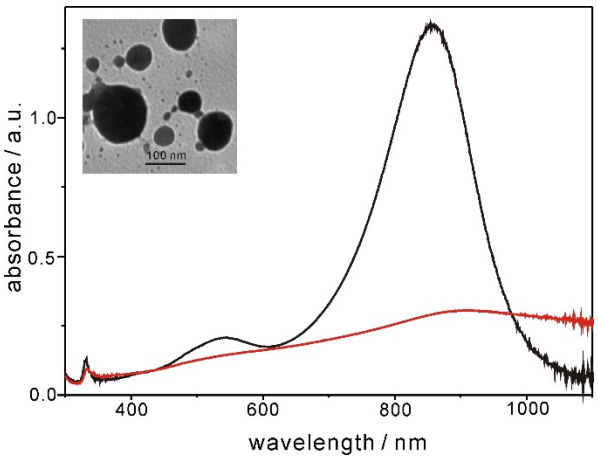

Figure 2-S3. Absorption spectra of PPy-free AgPRs in (black) water and (red) ethanol. The inset TEM image shows PPy-free AgPRs, which were dispersed in ethanol prior to TEM loading.

2.8. References

[1] S. Mao, G. Lu, K. Yu, Z. Bo and J. Chen, *Adv. Mater.*, 2010, **22**, 3521-3526.

[2] M. A. Mahmoud, *Langmuir*, 2013, **29**, 6253-6261.

[3] J. Lee and D.-J. Jang, *J. Phys. Chem. C*, 2016, **120**, 4130-4138.

[4] J. Sun, H. Wu and Y. Jin, *Nanoscale*, 2014, **6**, 5449-5457.

[5] Y. Bae, N. H. Kim, M. Kim, K. Y. Lee and S. W. Han, *J. Am. Chem. Soc.*, 2008, **130**, 5432-5433.

[6] S. Xing, L. H. Tan, M. Yang, M. Pan, Y. Lv, Q. Tang, Y. Yang and H. Chen, *J. Mater. Chem.*, 2009, **19**, 3286-3291.

[7] H. Jia, X. Bai and L. Zheng, *CrystEngComm*, 2012, **14**, 2920-2925.

[8] M. Yang, G. Chen, Y. Zhao, G. Silber, Y. Wang, S. Xing, Y. Han and H. *Phys. Chem. Chem. Phys.*, 2010, **12**, 11850-11860.

[9] D. Baranov, L. Manna and A. G. Kanaras, *J. Mater. Chem.*, 2011, **21**, 16694-16703.

[10] D. Fava, Z. Nie, M. A. Winnik and E. Kumacheva, *Adv. Mater.*, 2008, **20**, 4318-4322.

[11] Z. Nie, D. Fava, E. Kumacheva, S. Zou, G. C. Walker and M. Rubinstein, *Nat. Mater.*, 2007, **6**, 609-614.

[12] Z. Nie, D. Fava, M. Rubinstein and E. Kumacheva, *J. Am. Chem. Soc.*, 2008, **130**, 3683-3689.

[13] D. Aherne, D. E. Charles, M. E. Brennan-Fournet, J. M. Kelly and Y. K. Gun'ko, *Langmuir*, 2009, **25**, 10165-10173.

[14] J. Sun, X. Wang, J. Liu, P. Wan, Q. Liao, F. Wang, L. Luo and X. Sun, *RSC Adv.*, 2014, **4**, 35263.

[15] N. A. Hatab, C.-H. Hsueh, A. L. Gaddis, S. T. Retterer, J.-H. Li, G. Eres, Z. Zhang and B. Gu, *Nano Lett.*, 2010, **10**, 4952-4955.

[16] A. Kinkhabwala, Z. Yu, S. Fan, Y. Avlasevich, K. Müllen and W. Moerner, *Nat. Photonics*, 2009, **3**, 654-657.

[17] D. A. Rosen and A. R. Tao, *ACS Appl. Mater. Inter.*, 2014, **6**, 4134-4142.

[18] M. Stavytska-Barba, M. Salvador, A. Kulkarni, D. S. Ginger and A. M. Kelley, *J. Phys. Chem. C*, 2011, **115**, 20788-20794.

[19] X. Geng, W. Leng, N. A. Carter, P. J. Vikesland and T. Z. Grove, *J. Mater. Chem. B*, 2016, **4**, 4182-4190.

[20] B. Xue, D. Wang, J. Zuo, X. Kong, Y. Zhang, X. Liu, L. Tu, Y. Chang, C. Li, F. Wu, Q. Zeng, H. Zhao, H. Zhao and H. Zhang, *Nanoscale*, 2015, **7**, 8048-8057.

[21] J.-Y. Kim and J.-S. Lee, *Chem. Mater.*, 2010, **22**, 6684-6691.

[22] M. Lin, C. Guo, J. Li, D. Zhou, K. Liu, X. Zhang, T. Xu, H. Zhang, L. Wang and B. Yang, *ACS Appl. Mater. Inter.*, 2014, **6**, 5860-5868.

[23] M. Roca, N. H. Pandya, S. Nath and A. J. Haes, *Langmuir*, 2009, **26**, 2035-2041.

[24] M. Son, S. Jeong and D.-J. Jang, *J. Phys. Chem. C*, 2014, **118**, 5961-5967.

[25] S. Zhou, M. Wang, X. Chen and F. Xu, *ACS Sustain. Chem. Eng.*, 2015, **3**, 3346-3354.

[26] Y. Ren, J. Wang, X. Huang and J. Ding, *Electrochim. Acta*, 2015, **186**, 345-352.

[27] J. Wu, X. Zhang, T. Yao, J. Li, H. Zhang and B. Yang, *Langmuir*, 2010, **26**, 8751-8755.

[28] X. Liu, L. Li, Y. Yang, Y. Yin and C. Gao, *Nanoscale*, 2014, **6**, 4513-4516.

[20] K. Mallik, M. Mandal, N. Pradhan and T. Pal, *Nano Lett.*, 2001, **1**, 319-322.

[29] S. Fujii, A. Aichi, K. Akamatsu, H. Nawafune and Y. Nakamura, *J. Mater. Chem.*, 2007, **17**, 3777-3779.

[30] N. R. Jana, T. K. Sau and T. Pal, *J. Phys. Chem. B*, 1999, **103**, 115-121.

[31] N. R. Janafi, Z. L. Wangl and T. K. Sau, *Curr. Sci.*, 2000, **79**, 1367-1369.

[32] R. B. Bjorklund, *J. Chem. Soc.,Faraday Trans.*, 1987, **83**, 1507-1514.

[33] S. Fujii, A. Aichi, K. Akamatsu, H. Nawafune and Y. Nakamura, *J. Mater. Chem.*, 2007, **17**, 3777-3779.

[34] A. H. Chen, K. Kamata, M. Nakagawa, T. Iyoda, H. Q. Wang and X. Y. Li, *J. Phys. Chem. B*, 2005, **109**, 18283-18288.

[35] Q. Zhang, N. Li, J. Goebl, Z. Lu and Y. Yin, *J. Am. Chem. Soc.*, 2011, **133**, 18931-18939.

[36] X. Feng, H. Huang, Q. Ye, J.-J. Zhu and W. Hou, *J. Phys. Chem. C*, 2007, **111**, 8463-8468.

[37] T. Prathna, N. Chandrasekaran, A. M. Raichur and A. Mukherjee, *Coll. Surf. B*, 2011, **82**, 152-159.

[38] X. Cao, Y. Habibi and L. A. Lucia, *J. Mater. Chem.*, 2009, **19**, 7137-7145.

[39] X. Liang, Z. Wen, Y. Liu, X. Wang, H. Zhang, M. Wu and L. Huang, *Solid State Ionics*, 2011, **192**, 347-350.

[40] L. Liu and T. L. Kelly, *Langmuir*, 2013, **29**, 7052-7060.

Appendicies

A.1. List of Publications

1. Myounghee Son, **Sugyeong Jeong**, and Du-Jeon Jang, "Laser-Induced Nanowelding of Linearly Assembled Gold Nanorods to Fabricate Au@SiO_2 Core-Shell Nanowires" J. Phys. Chem. C, 2014, 118, 5961-5967.
2. Dongki Lee, **Sugyeong Jeong**, Jung-Hwa Park, Soo Young Park, and Du-Jeon Jang, "Effects of Gold Nanorods on the Excited-State Dynamics and Photovoltaic Performances of Hybrid Nanocomposites Containing Poly(3-hexylthiophene)" J. Mater. Sci., 2016, 51, 9669-9678.
3. **Sugyeong Jeong**, Dongki Lee, Joon Ki Kim, and Du-Jeon Jang, "Colloidal System of Polythiophene-Grafted Edge-Gold-Coated Silver Nanoprisms with Enhanced Optical Properties and Stability" New J. Chem., 2017, DOI: 10.1039/C6NJ02868C
4. Dong-Won Jeong, **Sugyeong Jeong**, and Du-Jeon Jang, "One-Step Polypyrrole Coating of Self-Assembled Silver Nanoprisms for Enhanced Stability and Raman Scattering" to be submitted.

A.2. List of Presentations

1. **Sugyeong Jeong**, and Du-Jeon Jang, "Fabrication of Au@SiO_2 Core-Shell Nanowires from Linearly Assembled and Silica-Coated Gold Nanorods", *The 113th Spring Meeting of the Korean Chemical Society*, Goyang, Korea (**2014**).

2. Dongki Lee, **Sugyeong Jeong**, and Du-Jeon Jang, "Facile Fabrication and Time-Resolved Emission Study of Poly(3-hexylthiophene)-Grafted Gold Nanorods", *The 115th Spring Meeting of the Korean Chemical Society*, Goyang, Korea (**2015**).

3. **Sugyeong Jeong** and Du-Jeon Jang, "Fabrication and Relaxation Dynamics of Poly(3-hexylthiophene)-Grafted Gold-Silver Nanoprisms", *The 117th Spring Meeting of the Korean Chemical Society*, Goyang, Korea (**2016**).

Abstract (Korean)

전도성 고분자로 표면 코팅된 귀금속 나노삼각형 구조체의 제조 방법, 물성 분석, 안정성 및 광학적 특성을 물리화학 및 재료화학 관점에서 연구하였다.

제 1장에서는 모서리 부분이 금 코팅된 은 나노삼각형을 전도성 고분자인 Poly(3-hexylthiophene) (P3HT)로 표면 개질하여 유기용매상에서도 높은 안정성을 보이며 특이한 광학 특성을 보이는 나노컴파짓을 합성했다. 흡수 및 발광 스펙트라를 통해 P3HT가 금 코팅된 은 나노삼각형에 흡착함으로써 광학 특성이 달라짐을 확인했고, 레이저 분석을 통해 P3HT내에 들뜬 전자의 소멸 시간이 금 코팅된 은 나노삼각형으로 에너지 전이하기 때문에 짧아지는 것을 확인했다. 또한, 삼중항으로 전이된 전자들은 P3HT가 나노삼각형 표면에 흡착함에 따라 그 소멸 시간이 길어짐을 측정하였다. 금 코팅된 은 나노삼각형의 뾰족한 모서리는 주변에 높은 전자기장을 유도하고, 이로 인해 입자와 입자 사이에 전자기장이 집중되어 핫스팟을 형성하여 P3HT의 라만 신호의 증가를 관찰 하였다. 합성한 나노컴파짓에 경우 강한 산화제에 대해 상대적으로 높은 안정성을 보이는 것을 확인 할 수 있었다.

제 2장에서는 자기조립된 은 나노삼각형 구조체 주변을 Pyrrole의 중합반응을 유도하여 Polypyrrole로 코팅시키고, 이에 대한 메커니즘, 안정성 및 광학 특성에 대해 분석하였다. 본 연구에서는 Pyrrole을 은 나노삼각형 구조의 자기조립 유도시를 위해 사용함과 동시에 코팅물질로 사용하여 구조체가 강한 산화제나 유기용매상에서 높은 안정성을 띠게 하였다. 또한, {111} 은 나노삼각형 표면에 선택적으로 흡착하는 Citrate 분자의 농도를 변화하여 자기조립 정도를 조절하였다. 자기조립 되고 Polypyrrole로 코팅된 은 삼각형 입자들은 강한 산화제에 비교적 높은 안정성을 보였다. 자기조립 정도가 높을수록 나노삼각형 입자들 사이에 전자기장이 집중되는 핫스팟 영역을 많이 형성하기 때문에 상대적으로 높은 Raman 신호를 얻을 수 있었다.

주요어: 광학 특성, 귀금속, 라만 산란, 안정성, 은 나노삼각형, 자기조립, 전도성 고분자

학번: 2014-21225